

Copyright Warning & Restrictions

The copyright law of the United States (Title 17, United States Code) governs the making of photocopies or other reproductions of copyrighted material.

Under certain conditions specified in the law, libraries and archives are authorized to furnish a photocopy or other reproduction. One of these specified conditions is that the photocopy or reproduction is not to be “used for any purpose other than private study, scholarship, or research.” If a user makes a request for, or later uses, a photocopy or reproduction for purposes in excess of “fair use” that user may be liable for copyright infringement,

This institution reserves the right to refuse to accept a copying order if, in its judgment, fulfillment of the order would involve violation of copyright law.

Please Note: The author retains the copyright while the New Jersey Institute of Technology reserves the right to distribute this thesis or dissertation

Printing note: If you do not wish to print this page, then select “Pages from: first page # to: last page #” on the print dialog screen

The Van Houten library has removed some of the personal information and all signatures from the approval page and biographical sketches of theses and dissertations in order to protect the identity of NJIT graduates and faculty.

ABSTRACT

PLASMA ENHANCED CHEMICAL VAPOR DEPOSITION OF STRESS FREE TUNGSTEN FILMS

by
David Perese

This study focuses on PECVD to make tungsten film for X-ray absorber for use in X-ray lithography applications. The previous LPCVD study was used for comparison of film properties. A cold wall, single wafer, Spectrum 211 CVD reactor was used for the deposition of tungsten from H_2 and WF_6 . The growth kinetics were determined as a function of temperature, pressure and flow rate ratio. The deposition rate was found to follow an Arrhenius behavior between 300-500°C with an activation energy of 55.7 kJ/mol. The growth rate increased linearly with total pressure and H_2 partial pressure. In the H_2/WF_6 ratio studies growth rate increased up to flow ratio of 10 followed by saturation. The as-deposited film stress is strongly dependent on deposition temperature with a weak relationship with pressure and flow ratio. The resistivity showed no parameter dependency, with the films having preferred orientation of the (200) plane. Plasma enhanced CVD was used for the deposition of tungsten film from the same precursors and the same Spectrum 211 CVD reactor under the same deposition parameter range used in the LPCVD study for temperature, pressure, and WF_6 and H_2 flow rates, RF plasma power was varied. Zero stress was achieved at RF power of 400W, 600°C, 500 mTorr, WF_6 and H_2 flow rates at 5 and 100 sccm respectively. In addition, resistivity values were as low or lower than those reported in the LPCVD study.

**PLASMA ENHANCED CHEMICAL VAPOR DEPOSITION OF STRESS FREE
TUNGSTEN FILMS**

by
David Perese

**A Thesis
Submitted to the Faculty of
New Jersey Institute of Technology
in Partial Fulfillment of the Requirements for the Degree of
Master of Science in Engineering Science
Interdisciplinary Program in Materials Science and Engineering
May 1996**

APPROVAL PAGE

PLASMA ENHANCED CHEMICAL VAPOR DEPOSITION OF STRESS FREE
TUNGSTEN FILMS

David Perese

Dr. Roland A. Levy, Thesis Advisor
Professor of Physics,
Director of Materials Science and Engineering Program, NJIT

/ / / / / Date

Dr. Lev N. Krasnoperov,
Professor of Chemical Engineering, Chemistry, and
Environmental Science, NJIT

/ / / / / Date

Dr. N.M. Ravindra,
Professor of Physics,
Associate Director, Electronic Imaging Center, NJIT

/ / / / / Date

BIOGRAPHICAL SKETCH

Author: David Perese

Degree: Master of Science in Engineering Science

Date: May 1996

Undergraduate and Graduate Education:

- Master of Science in Engineering Science,
New Jersey Institute of Technology,
Newark, New Jersey, 1996
- Bachelor of Science in Electrical Engineering,
Fairleigh Dickinson University,
Teaneck, New Jersey, 1990

Major: Materials Science and Engineering

ACKNOWLEDGMENT

The author wishes to express his sincere gratitude to his advisors, Dr. Roland A. Levy for his guidance, friendship, moral and financial support throughout this thesis work, without which it would not have been completed. Special thanks to Dr. N.M. Ravindra and Dr. Lev N. Krasnoperov for serving as members of the committee.

The author appreciates the timely help and suggestions from the CVD Lab. members, including: Mahalingam Bhaskaran, Jan Opyrchal, Lan Chen, Manish Narayan, Emmanuel Ramos and especially to Vitaly Sigal for his invaluable technical assistance, co-worker Hong Yu Chen who provided assistance on all aspects of this project, Chenna Ravindranath and Majda Newman who provided the X-ray diffraction data.

TABLE OF CONTENTS

Chapter	Page
1.1.1 The Promising Application of X-ray Lithography.....	1
1.1.2 X-ray Mask.....	2
1.1.3 The Development of Low Stress Tungsten film.....	5
1.1.3.1 Kinds of Stress in Thin Film.....	5
1.1.3.2 Low Stress Tungsten Film by PVD.....	6
1.1.3.3 Low Stress Tungsten Film by CVD.....	6
1.2 Chemical Vapor Deposition.....	7
1.2.1 Basic Steps of CVD.....	7
1.2.2 Experimental Parameters in CVD.....	8
1.2.2.1 Deposition Temperature.....	8
1.2.2.2 Gas Pressure.....	10
1.2.2.3 Gas Flow Rate.....	11
1.2.3 Types of CVD Processes.....	12
1.2.3.1 Classification of Process Types.....	12
1.2.3.2 Thermally Activated Atmospheric Pressure Processes (APCVD)..	13
1.2.3.3 Thermally Activated Low Pressure Processes (LPCVD).....	14
1.2.3.4 Plasma-Enhanced Deposition Process (PECVD).....	15
1.2.3.4.1 Principles of Plasma Enhanced CVD Deposition.....	15
1.2.3.4.2 Characteristics of the Plasma CVD Process.....	17
1.2.3.4.3 Variables of Plasma Process.....	18
1.2.3.4.4 Advantages of PECVD.....	19
1.2.3.4.5 Limitations of PECVD.....	20
1.2.3.4.6 Applications of Plasma CVD.....	21

TABLE OF CONTENTS
(Continued)

Chapter	Page
1.2.3.5 Photo-Enhanced Chemical Vapor Deposition.....	22
1.2.3.6 Laser-Enhanced Chemical Vapor Deposition (LCVD).....	22
1.3 Chemical Vapor Deposition of Tungsten.....	23
1.3.1 Tungsten Film Application.....	23
1.3.2 Reaction for CVD of Tungsten.....	24
1.3.2.1 Reduction of WF_6 with Si.....	25
1.3.2.2 Reduction of WF_6 with H_2	27
1.3.2.3 Reduction of WF_6 with SiH_4	30
1.3.2.4 The Dissociation of $W(CO)_6$	33
1.4 Plasma Enhanced Chemical Vapor Deposition of Tungsten Films.....	34
1.4.1 PECVD Tungsten Film Overview.....	34
1.4.2.1 PECVD Reduction of WF_6 with H_2	35
2 THE DEPOSITION PROCESS OF TUNGSTEN THIN FILM.....	38
2.1 Reaction System.....	38
2.1.1 Equipment Set up.....	38
2.1.2 Pre-deposition Preparation.....	39
2.1.2.1 Leak Check.....	39
2.2 Experimental Procedure.....	40
2.2.1 Wafer Preparation and Transport.....	40
2.2.2. Film Deposition	40
2.3. Tungsten Film Characterization Techniques.....	41
2.3.1 Physical Property.....	41
2.3.1.1 Film Thickness.....	41

TABLE OF CONTENTS
(Continued)

Chapter	Page
2.3.2 Structure Property.....	42
2.3.2.1 X-ray Diffraction Analysis.....	42
2.3.3 Electrical Property.....	42
2.3.4 Mechanical Property.....	44
3 RESULTS AND DISCUSSION.....	46
3.1 The Effects of Deposition Variables on Film Deposition Rate.....	46
3.1.1 Temperature Dependent Study.....	46
3.1.2 Pressure Dependent Study.....	47
3.1.3 Flow Ratio Dependent Study.....	50
3.2 Tungsten Film Characteristics.....	51
3.2.1 Stress.....	51
3.2.1.1 Temperature Effect.....	52
3.2.1.2 Effect of PECVD on Stress.....	55
3.2.1.3 Pressure Effect.....	58
3.2.1.4 Flow Rate Ratio Effect.....	59
3.2.2 Resistivity.....	59
3.2.2.1 Resistivity of PECVD W Films.....	61
3.2.3 Crystal Orientation.....	64
3.2.3.1 Crystal Orientation of PECVD Films.....	66
4 CONCLUSIONS AND SUGGESTIONS.....	70
4.1 Conclusions and Suggestions-PECVD Study.....	72
5 REFERENCES.....	74

LIST OF TABLES

Table	Page
1 Temperature Effect on Reaction by Thermodynamic Consideration.....	10
2 Free Energy Changes at 600K.....	26
3 The Detailed Sub-step in the Pre-purge and Post-purge Step.....	41
4 X-ray Diffraction Lines for α -W from Random Tungsten Powder.....	67

LIST OF FIGURES

Figure	Page
1.1 Temperature Dependence of Growth Rate for CVD Films.....	9
1.2 Idealized Growth-rate versus Fluid Flow-rate Plot Showing the Different Growth Regimes.....	13
1.3 Schematic for Applications of Blanket and Selective Metal CVD for Microelectronics Applications.....	24
2.1 Schematic Diagram of the Chamber.....	39
2.2 Four-point Probe System for Sheet Resistance Measurement.....	44
2.3 The Resistivity Measurement Position on the Wafer.....	45
2.4 Optical System for Stress Measurement Setup.....	34
3.1 Variation of Growth Rate as a Function of Temperature at a Constant Total Pressure, WF ₆ Flow Rate, and H ₂ /WF ₆ Ratio.....	47
3.2 Variation of Growth Rate as a Function of Total Pressure at a Constant Temperature, WF ₆ Flow Rate, and H ₂ /WF ₆ Ratio.....	49
3.3 Variation of Growth rate as a Function of H ₂ Partial Pressure at a Constant Temperature, WF ₆ Flow Rate, and H ₂ /WF ₆ Ratio.....	50
3.4 Variation of Growth Rate as a Function of Flow Ratio at a Constant Temperature, Pressure, and WF ₆ Flow Rate.....	51
3.5 Variation of Stress as a Function of Temperature at a Constant Pressure, WF ₆ Flow Rate, and H ₂ /WF ₆ Ratio.....	52
3.6 Variation of ϵr^{-1} as a Function of Reciprocal Temperature.....	56
3.7 Variation of Stress as a Function of Temperature at Constant RF Plasma Power, Pressure, WF ₆ Flow Rate, and H ₂ /WF ₆ Flow Rate Ratio.....	57
3.8 Variation of Stress as a Function of RF Plasma Power at Constant Temperature, Pressure, WF ₆ Flow Rate, and H ₂ /WF ₆ Flow Rate Ratio.....	57
3.9 Variation of Stress as a Function of Pressure at a Constant Temperature, WF ₆ Flow Rate, and H ₂ /WF ₆ Ratio.....	58
3.10 Variation of Stress as a Function of Flow Ratio at Constant Temperature, Pressure and WF ₆ Flow Rate.....	59
3.11 The Dependent Behavior of Resistivity of CVD W on Temperature.....	61

LIST OF FIGURES
(Continued)

Figure	Page
3.12 The Independent Behavior of Resistivity of CVD W on Total Pressure.....	62
3.13 The Independent Behavior of Resistivity of CVD W on Flow Ratio.....	62
3.14 Resistivity as a Function of RF Plasma Power.....	63
3.15 Resistivity as a Function of Temperature.....	63
3.16 Temperature Effect on Texture Coefficient of (200) Plane.....	67
3.17 Pressure Effect on Texture Coefficient of (200) Plane.....	68
3.18 Flow Ratio Effect on Texture Coefficient of (200) Plane.....	68
3.19 RF Plasma Power Effect on Texture Coefficient of (200) Plane.....	69
3.20 Temperature Effect on Texture Coefficient of (200) Plane of Plasma Films..	69

CHAPTER 1

INTRODUCTION

1.1 Tungsten-One of the Most Desirable X-ray Absorbers

X-ray lithography is a promising technique for replicating sub-micron patterns of large area[1]. One of the key factors in X-ray lithography is the construction of the mask. This is because the resolution and accuracy of X-ray lithography is determined by the X-ray mask. The mask essentially consists of absorber patterns and a thin mask substrate. Among many absorbers, tungsten is the most promising material not only because of its high X-ray absorption, but also because of its low thermal expansion, high Young's modulus and its refractory properties. However, it is difficult to control the stress in the tungsten film. This study focuses on plasma enhanced chemical vapor deposition (PECVD) of low stress tungsten film in an attempt to achieve stress free membranes. In this chapter, the importance of the X-ray mask for X-ray lithography is presented. Then the importance of low stress in X-ray absorber is justified followed by a discussion of the general concepts of CVD (Chemical Vapor Deposition) focusing on the principles of PECVD. Finally, a systematic review of the development of PECVD tungsten is presented.

1.1.1 The Promising Application of X-ray Lithography

Lithography is one of the most important technologies in the mass production of microelectronic circuits[2]. More is spent for lithographic systems than for any other type of IC processing equipment in a production line. Lithography has allowed the development of the ever-smaller and faster, more-able, and less-expensive electronic devices, which have been reshaping our world for 30 years. The trend towards smaller-feature size devices will not stop until some fundamental limit is encountered in device operation, or fabrication costs increase radically with the reduction in feature size. Optical lithography has made great strides in providing smaller and smaller structures, but it presently appears that the practical resolution limit using near-U.V. coherent sources is larger than $0.3 \mu\text{m}$. This limit is determined by diffraction effects and practical limits on lens systems. To permit the transition to smaller details some methods have been developed that use electrons or ions instead of light. The effective wavelength of these particles is much smaller than the dimensions of the details required, so that diffraction effects are no longer a problem. Another promising method for VLSI is X-ray lithography, in which X-rays are used to produce an image of the mask pattern on a slice coated with X-ray sensitive resist. The wavelength of the radiation varies from about 0.5 to 3nm, so that no diffraction effects occur. As compared with the electron method, X-ray lithography at these wavelengths has the advantage that there is no proximity effect[3].

1.1.2 X-ray Mask

The major effort in X-ray lithography is focused on the development of an appropriate mask technology. Considering the progress in all other elements of X-ray lithography, the successful industrial application of this new technology will depend primarily on whether the remaining problems in mask technology can be solved. The X-ray mask consists of a thin membrane of low-Z material carrying a high-Z absorber pattern[4]. The requirements for X-ray mask quality are rigid and cannot be compromised. For the membrane material, such requirements include[5]:

- high X-ray transmission ($>80\%$ at 0.4-1.5nm)
- adequate optical transmission ($>60\%$ at 633nm)
- high modules of elasticity ($>10^{11}$ Pa)
- low stress ($<5 \times 10^8$ dynes cm^{-2})
- low defect density (0.1cm^{-2})
- long lifetime ($>10^6$ exposures at a flux of 100mw cm^{-2})
- radiation hardness ($<10 \text{nm}$ distortions at absorbed does $>10^3 \text{kJ cm}^{-3}$)
- low cost (\$5,000)

For the absorber, such requirements include:

- high x-ray absorption ($>99\%$ at 0.4-1.5 nm)
- low stress ($<5 \times 10^8$ dynes cm^{-2})
- low defect density ($<0.1 \text{cm}^{-2}$)
- minimal feature distortion ($<50 \text{nm}$)
- ease of pattern

Among the numerous X-ray mask membranes considered, four have emerged as most promising. These are silicon, silicon nitride, silicon carbide and boron nitride. Silicon, a more versatile material, has been used with both Au and W as the absorber material[6]. In this study W was deposited on the Si wafer which is a promising membrane material and is easily available.

In X-ray lithography, pattern features on the mask should not deviate from their assigned in-plane positions by more than a fraction of the minimum line width. In an X-ray lithography mask, such distortion can arise if the absorber, which is in relief on the mask membrane, has non zero internal stress. Absorber stress exerts a torque on the membrane at the edges of features, and this leads to out-of-plane and in plane distortion. Therefore, to reduce distortion to acceptable levels one must achieve near-zero internal stress [7]. Since the X-ray lithography was first developed, Au(gold) has been used as an X-ray mask absorber. This is because that the Au has a high absorption coefficient, and the internal stress of Au film can be easily controlled by selecting the deposition condition. However, it is known that the stress in gold changes with time, even at room temperature[8]. Moreover, Au cannot be dry etched and its thermal expansion coefficient ($14.2 \times 10^{-6} \text{ K}^{-1}$) is much larger than that of mask membranes such as Si ($2.6 \times 10^{-6} \text{ K}^{-1}$) and SiC ($3.8\text{-}4.2 \times 10^{-6} \text{ K}^{-1}$). Tungsten (W) is an attractive alternative to Au because it is refractory, can be dry etched in fluorine-containing gases and has a much lower thermal expansion coefficient ($4.5 \times 10^{-6} \text{ K}^{-1}$) than gold[9]. Moreover, it absorbs more effectively than gold(and may further reduce the aspect ratio requirements). However, there are several problems associated with W: (1) its internal stress is a strong function of

deposition parameters and hence achieving zero stress can be problematic [10]; (2) there is a metastable phase of W, β -W, which can be incorporated in deposited films. The β -W can transform to the stable phase α -W and, in the process, change the net stress[11] , and (3) the high electron backscattering from W may increase the difficulty of patterning.

1.1.3 The Development of Low Stress Tungsten Film

1.1.3.1 Kinds of Stress in Thin Film: The total stress in a film is the sum of: (a) the thermal stress, resulting from the difference in the coefficient of thermal expansion between the film and the substrate; (b) the intrinsic stress, which originates from the change in the film structure.

The thermal stress caused by the difference in thermal expansion coefficients (α) between film and substrate. After cooling from deposition temperature (T) to room temperature (T_o), the biaxial thermal stress(σ_{th}) in a film on a substrate is obtained from

$$\sigma_{th} = \frac{E_f}{1-\nu_f} \int_{T_o}^T \Delta\alpha (T') dT \quad (1.1)$$

where E_f is young's modules and ν_f is the Poisson constant of the film. For the case of tungsten film, $E_f = 410$ GPa and $\nu_f = 0.28$. Since the average linear thermal expansion coefficients between 20 and 500°C for W and SiC amount to 4.6 and 4.2×10^{-6} K⁻¹ respectively, the thermal stress due to cooling is only $0.23 \times \Delta T$. The thermal stress is very small, the high residual stress values are ascribed to intrinsic stress.

The stress present in the absence of thermal effects are usually called intrinsic stresses or, more appropriately, growth stress. Such stresses are associated with the growth of a film on a substrate.

1.1.3.2 Low Stress Tungsten Film by PVD: In literature of tungsten film for X-ray absorber application deposition by PVD prevails. However, tungsten films deposited by PVD (i.e., sputtering, evaporation) have large stress. To reduce the stress in the PVD tungsten film, some methods were suggested, which include:

(1) Ion implantation

Yao C, et al. [12] reduce the stress in tungsten film by using Si ion implantation to a projected range of 10nm in the W at doses in the range of 10^{15} - 10^{16} cm^{-2} . Distortion correction takes place because the implantation produces compressive stress near the upper surface, resulting in a torque that balances a torque of opposite sign at the absorber-membrane interface due to tensile stress in the tungsten.

H. Luethje et al. [13] reported effective stress reduction ($\sigma < 10^7$ N/m^2) and excellent long term stability ($\Delta\sigma < 5 \times 10^6$ N/m^2) are being obtained by sputtering the 0.8 μm thick tungsten layers in the presence of oxygen, and subsequently annealing them in an oxidizing atmosphere.

(2) Tungsten alloy

Yoshioka, et al. [14] investigated W-Ti alloy as x-ray mask absorber. The W-Ti film were deposited by sputtering the W-Ti (1 wt% Ti content) target using Ar+N₂ gas

with a DC magnetron sputtering system. They obtained the low stress tungsten film which is satisfactory for an X-ray mask absorber.

1.1.3.3 Low Stress Tungsten Film by CVD: There are reports about low stress tungsten film by CVD for interconnect or plug application in VLSI technology. Up to now, no report about W CVD film for X-ray absorber application was found. In a later review of CVD tungsten, we will discuss low stress W film by CVD.

1.2 Chemical Vapor Deposition

Chemical vapor deposition(CVD) is one of the most important methods of film formation used in the fabrication of very large scale integrated (VLSI) silicon circuits, as well as of microelectronic solid state devices in general. In this process, chemicals in the gas or vapor phase are reacted at the surface of a substrate where they form a solid product[15].

1.2.1 Basic Steps of CVD

A CVD process basically is a type of surface catalysis process since the deposition process is thermodynamically favorable and takes place on the substrate surface. Most of the time the surface serve as a catalyst for the reactions leading to amorphous deposition and crystal growth. The same sequence of events in a heterogeneous reaction can therefore be applied to crystal growth by CVD[16] . These events are:

- (a) a given composition (and flow rate) of reactant gases and diluent inert gases is introduced into a reaction chamber.

- (b) then gaseous species diffuse to the substrate.
- (c) the reactants are adsorbed on the substrate.
- (d) the adsorbed reactants undergo migration and film forming chemical reactions.
- (e) the gaseous by-products of the reaction are desorbed.
- (f) gaseous transport of by-products.
- (g) bulk transport of by-products out of reaction chamber.

1.2.2 Experimental Parameters in CVD

Any one of the several steps taking place in a CVD process can be the rate-determining step. A number of experimental parameters play an important role in determining or altering the rate-determining step. The experimental parameters, which are discussed individually below are: deposition temperature, reactant partial pressure, gas flow rate.

1.2.2.1 Deposition Temperature: The rate of product deposition is dependent primarily on temperature. The rate controlling step in the process such as surface reaction, and surface diffusion can be described by the Arrhenius equation.

$$R=R_0\exp(-E_a/kT) \quad (1.2)$$

Activation energy signifies the presence of an energy barrier which must be overcome in order for the process to occur. Activation energies for most surface processes

are usually greater than 10 kcal/mole and lie in the range of 25-100 kcal/mol[16]. Conversely, mass transport phenomena such as diffusion are almost insensitive to temperature. Therefore, when plotted as an Arrhenius expression (the deposition rate vs the reciprocal temperature) to find activation energies, a preliminary distinction between the surface phenomena and the gas phase mass transport phenomena can be made by observing the temperature dependence of the process.

A typical Arrhenius plot exhibits two regions as shown in figure 1.1. At lower temperature, there is always enough supply of reactants to the surface and this supply is faster than the consumption of the reactants during reaction. Then the overall rate is controlled by the surface kinetics. At higher temperature, the rate is limited by the rate of

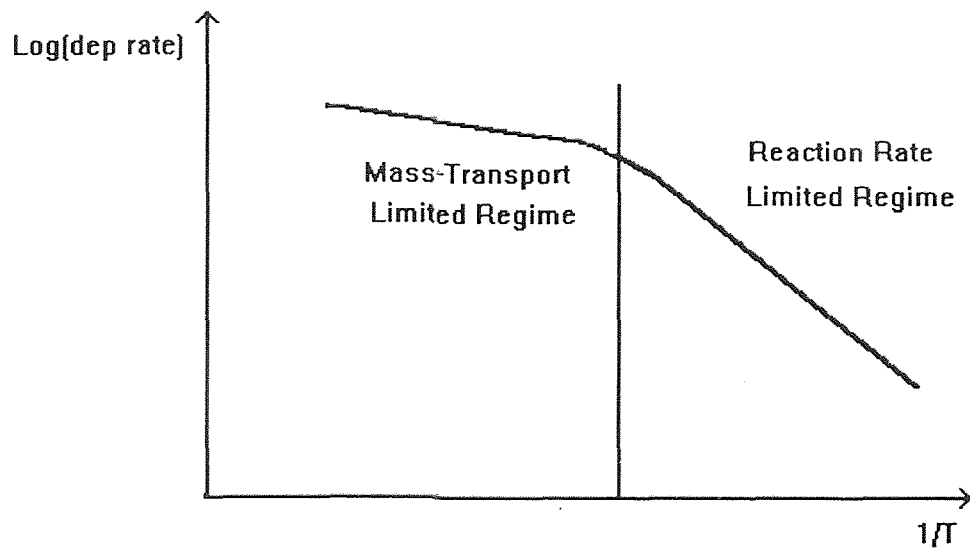


Figure 1.1 Temperature dependence of growth rate for CVD films

insufficient reactants supply although the rate of surface reaction is higher. It is possible to switch from one rate limiting step to the other by changing the temperature as shown in figure 1.1 [17].

Thermodynamic aspects of the reaction system should also be considered when examining the effect of deposition temperature. Assuming the process is near equilibrium, the temperature effect on deposition based on the thermodynamic considerations is presented in Table 1:

Table 1. Temperature effect on reaction by thermodynamic consideration

<p>From Van't Hoff's Equation</p> $d \ln K_p/dT = \Delta H/RT^2$ <p>If $\Delta H > 0$ and T is increasing</p> <ol style="list-style-type: none"> a. K_p increases b. Reaction shifts to right c. Deposit product increases e. A cold wall reactor with rf-heated substrate is needed

1.2.2.2 Gas Pressure: Surface reactions involving single adsorbed molecules are classified as unimolecular reaction[18]. This can be treated by Langmuir adsorption isotherm. Let θ be the fraction of surface that is covered and $1-\theta$ the fraction that is bare.

The rate of adsorption is then $k_1P(1-\theta)$, where P is the gas pressure and k_1 is proportionality constant. The rate of desorption is $k_{-1}\theta$. At equilibrium, the rates of adsorption and desorption are equal, so that

$$\frac{\theta}{1-\theta} = \frac{k_1}{k_{-1}} P = KP \quad (1.3)$$

where K , equal to k_1/k_{-1} , is the adsorption equilibrium constant. The equation can be written as

$$\theta = \frac{KP}{1+KP} \quad (1.4)$$

The rate of reaction is proportional to θ and may therefore be written as

$$D.R. = k_2\theta = \frac{k_2KP}{1+KP} = k_0 \cdot e^{\frac{-E_a}{RT}} \frac{KP}{1+KP} \quad (1.5)$$

where k_0 is the proportionality constant at certain temperature. This is the simplest treatment of surface reaction.

1.2.2.3 Gas Flow Rate: When growth rate for a CVD process is plotted as a function of reactant gas flow rate, the generalized form of the relationship is shown in figure 1.2 [19].

At very small flow rate (region 1), the incoming gas stream has sufficient residence time

to equilibrium with the substrate surface. Increasing the total flow rate increases the rate of reactant input, and thus more material per unit time equilibrates with the substrate surface. The rate increases linearly with total flow rate in this region[20].

When the flow rate is increased above a certain point, the entire gas stream no longer has sufficient residence time for complete equilibrium (region 2). At this point, a portion of the incoming reactants pass by unreacted. This gives higher bulk stream partial pressures than the surface partial pressure. Then the rate-limiting process is diffusion from the main gas stream to the substrate surface. It is known that the boundary layer thickness, where the diffusion process takes place, is inversely proportional to the square root of the gas velocity[21]. Then, in this regime, the surface reaction shows a square root dependence on the gas flow rate.

At high flow rate, the reaction rate reaches a plateau (region III) and becomes independent of flow rate[22]. Here the reaction rates are so slow relative to the gas flow and mass transfer rates that the partial pressure at the surface becomes essentially the input partial pressure. Then the process is said to be 'kinetically controlled'. The reactant flow rate for kinetics studies should be in this plateau regime so that the true temperature and partial pressure dependence of the reaction can be observed.

1.2.3 Types of CVD Processes

1.2.3.1 Classification of Process Types: CVD processes can be classified according to the type of energy supplied to initiate and sustain the reaction: (i) Thermally activated reactions at various pressure ranges, which comprise the vast majority of CVD processes;

heat is applied by resistance heating, rf induction heating, or infrared radiation heating techniques. (ii) Plasma promoted reactions, where an rf (or dc)-induced glow discharge is the source for most of the energy that initiates and enhances the rate of reaction. (iii) Photon induced reactions, where a specific wavelength radiation triggers and sustains the reaction by direct photolysis or by an energy transfer agent, such as uv-activated mercury.

1.2.3.2 Thermally Activated Atmospheric Pressure Processes (APCVD): The simplest CVD process type is conventional atmospheric or normal pressure CVD

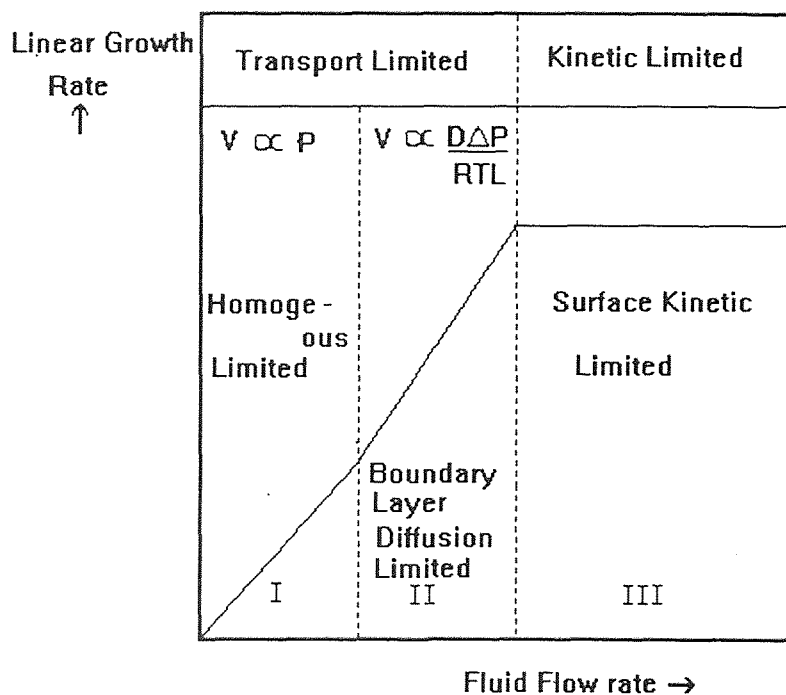


Figure 1.2 Idealized growth-rate versus fluid flow-rate plot showing the different growth regimes

(APCVD or NPCVD)[23]. Reactant vapors or gases are introduced in the reactor at normal atmospheric pressure. The pressure in the reactor system is slightly above atmospheric due to the impedance of the gas flow at the exit part of the system. The temperature and reactant flow rate determine the rate of film deposition. Heat is supplied by resistance heating, by rf induction techniques, or by infrared radiation. The advantage of APCVD is its simplicity; no vacuum pumps are needed. The disadvantage is the tendency for homogeneous gas phase nucleation that leads to particle contamination, unless special optimized gas injection techniques are used.

1.2.3.3 Thermally Activated Low Pressure Processes (LPCVD): Low pressure CVD is widely used in the extremely cost competitive semiconductor industry for deposition films of insulators, amorphous and polycrystalline silicon, refractory metals, and silicides[24]. The gas pressure of ~ 0.5 to 1 Torr employed in LPCVD reactors distinguishes it from conventional CVD systems operating at 760 Torr. Lowering the gas pressure enhances the mass transfer rate relative to the surface reaction rate. The mass transfer of gases involves their diffusion across a slowly moving boundary layer adjacent to the substrate surface. The thinner this boundary layer and the higher the gas diffusion rate, the greater the mass transport that results. Although the boundary layer for LPCVD is thicker than that of APCVD, the diffusivity (D) for LPCVD is much higher than APCVD, thus, low pressure deposition conditions enhance mass transfer greatly, providing high wafer capacity, better thickness uniformity and less gas phase reactions, which are especially important in VLSI

processing where a very high device reliability and high product yield must be achieved[25]. The disadvantages are the relatively high operation temperature.

1.2.3.4 Plasma Enhanced Deposition Processes (PECVD): CVD or plasma-enhanced CVD combines a radio frequency-induced glow discharge process and low pressure CVD in which the reaction is activated by a plasma. Glow discharge creates a highly reactive chemical species generated from gaseous reactants which subsequently interact to form a thin solid film on the substrate surface[15,23,76]. Plasma CVD processes were developed in the 1960's at first for semiconductor applications notably due to the desire to replace silicon dioxide metal protection layers with silicon nitride. These nitride layers requires a temperature of approximately 660°C for a thermally activated CVD. This temperature causes enough problems with the underlying aluminum layers as to be unusable[23]. Plasma CVD process has been expanding ever since and is now used in a wide variety of CVD applications.

1.2.3.4.1 Principles of Plasma CVD Deposition: If the energy of a gas is increased to a high enough level, all gas molecules will be disassociated into atoms that are increasingly ionized (stripped of their electrons) forming a plasma consisting of positive ions, electrons and unionized (neutral) atoms. However, this requires a temperature >5000k. Plasma generated by combustion flame has a temperature limit of 3700k which is insufficient for complete ionization (approximately 10%).

A more efficient way to achieve the higher temperatures needed for more complete ionization is to apply either a high or low frequency electric field. When the electrical energy of a fixed amount of gas is increased complete ionization is achieved[76]. There are two types of plasmas employed in CVD. A low frequency (isothermal) plasma discharge exists when a low frequency electric field is applied to a gas, both electrons and the positive ions acquire energy and have their temperatures raised almost equally, so the plasma is in equilibrium (isothermal). These isothermal plasmas are generated at relatively high pressures (100 torr- 1atm.). The high pressure reduces the mean free path between colliding molecules, increasing the frequency of collisions between ions and molecules which are heated readily. For a typical example of this type of discharge, the arc discharge, requires a large amount of power (in the MW range) and are extremely hot. Therefore their applications have been limited in CVD deposition with the exception of diamond deposition.

The other type of plasma of major interest in CVD is non-equilibrium (non-isothermal) plasma (glow discharge). In this process the plasma is generated by a high frequency electric field at a lower pressure than isothermal plasma (< 2 torr). In the high frequency electric field, the gas molecules are ionized into positive ions and electrons. The electrons have a much lighter mass and higher mobility than other species and are quickly accelerated to high energy levels ($>5000\text{K}$ at an average energy between 1 and 10 eV.). Because of the very low mass they therefore do not appreciably increase the temperature of the plasma as a whole. The heavier ions however can not respond to the rapidly alternating electric field due to their inertia and do not have their energy and temperature

raised, in contrast to the low frequency process. (electron temp./gas temp. 10-100 [77]). Thus the plasma is in non-equilibrium (non-isothermal). The energy of these heavier species is $< .05$ eV. The high energy electrons then collide with the gas molecules resulting in dissociation into highly reactive chemical species (free radicals, ions, atoms, metastable species, excited molecules, photons[77]) which subsequently initiate the reaction. The efficiency of the ionization process is a function of the kinetic energy of the electrons, with the efficiency rapidly increasing between 10 and 100 eV. The electrons acquire energy directly from the applied electric field. The concentration of positive and negative charge carriers are approximately equal, with an electron (and positive ion) density range of 10^9 - 10^{12} / cm^3 . Glow discharge plasmas are weakly ionized with the ratio of neutral species to electrons or ions greater than 10^3 . Due to this higher concentration of neutral species it is primarily these species responsible for film formation[77]). The high frequency currents can be generated by a radio frequency (rf), ac, dc or microwave source. The vast majority of research and development employs an rf field as the means of plasma excitation because many of the films deposited are dielectrics where a dc source is not feasible. An rf source typically operates at 450 KHz or 13.45 Mhz and the microwave at 2.45 Ghz. For the rf source the reactor configuration consists of a parallel plate, cold wall reactor with two parallel electrodes with the substrate(s) serving as one of the electrodes, usually the grounded one while the other is powered.

1.2.3.4.2 Characteristics of the Plasma CVD Process: In addition to the generation of chemically reactive species via breaking of chemical bonds through electron/gas molecule

collisions, the other primary function of the plasma is to provide energetic radiation (primarily ions but also electrons and photons) for surface chemistry alteration[77]. Due to the difference in mobility between electrons and positive ions, the substrate surface initially assumes a negative potential with respect to the plasma. This in turn leads to a positive ion bombardment of the surface. The energy of the ions striking the surface is a function of the potential difference between the plasma and substrate, the number of collisions (related to gas pressure) and the rf frequency. These energies are usually greater than most bond strengths (up to 1000 eV) and can modify surface chemistry during deposition. Resulting phenomena that can result from plasma surface interaction includes the following: 1) surface cleaning and desorption of unwanted impurities during and/or after deposition due to ion bombardment. Sufficient particle energy will cause sputtering/etching of surface. 2) Creation of adsorption and nucleation sites is another development of impinging particles which can break chemical bonds. Finer-grained deposits will result, and the growth of unique phases are another possibility. 3) Increase in surface mobility of adsorbed species due to momentum transfer possibly resulting in increased step coverage 4) implantation of bombarding particles or recoil implantation of adsorbed species resulting in impurity incorporation and subsequent modification of surface properties and composition. 5) Generation of defects (vacancies, dislocations, interstitials, stacking faults, etc.) by particle bombardment.

1.2.3.4.3 Variables of Plasma Process: The major variables affecting film uniformity and deposition range are rf power density and distribution, gas phase composition and

distribution, and total pressure in the reaction zone[15]. The most important of these variables is distribution of power density. This is due to the very short lifespan of the reactive species, which must be continuously regenerated throughout the deposition zone. In general, the density of charged particles must be large enough so that significant coulombic interaction occurs. It is this interaction that creates the fluidlike nature of the plasma which determines much of its properties[71]. Most applications for plasma deposition use a temperature range between approximately 200 - 400° C at system pressures of 0.1 - 2 Torr.

1.2.3.4.4 Advantages of PECVD: The major advantage of plasma CVD is the ability to produce deposition processes that would normally occur only at much higher temperatures with LPCVD[15,23,71,76-77]. As explained above, the generation of reactive chemical species is done at gas temperatures near ambient due to the non-isothermal nature of the plasma. Therefore many high temperature reactions can be made on temperature-sensitive substrates at low temperatures. Examples are aluminum, which would melt at the required LPCVD temperature, organic polymers which would otherwise degrade and outgas, or metals and alloys which would undergo structural changes at higher temperatures. Dopants for semiconductors (boron, phosphorus) can readily diffuse between buried layers of the device if the temperature exceeds 800° C with damaging effects to the semiconductor properties[76]. Other advantages of the plasma process is that deposition rates are usually increased. With the low pressures used, the rate controlling regime is surface kinetics leading to greater film uniformity. Low

temperatures are more conducive to the growth of amorphous or fine-grained polycrystalline films. The number of deposition parameters necessary to alter film characteristics are available with PECVD for “tailoring” of these properties[77].

1.2.3.4.5 Limitations of PECVD: Deposits of pure materials are often difficult to achieve. Low temperatures during deposition in many cases results in incomplete desorption of byproducts and other gases, particularly hydrogen, resulting in unwanted inclusions and outgassing causing thermal instability. An example of this phenomena is hydrogen given off from plasma nitride films that may cause damaging effects on the electronic properties of certain devices[15]. The complexity of reactions makes stoichiometric compounds difficult to achieve, as in the case with carbides, nitrides, silicides and oxides. While usually detrimental to film properties and lowers its resistance to chemical etching and radiation, such alterations can be beneficial in certain applications, i.e. improved optoelectronic properties of amorphous silicon used in solar cells when hydrogen is present[76]. Another disadvantage is potential damage to fragile substrates such as in ULSI and some III-V and II-VI semiconductor materials due to ion bombardment if the ion energy exceeds 20 eV. In addition, the plasma will react strongly to the surface as deposition takes place meaning that the deposition rate and many film properties will be a function of the plasma uniformity. More fully exposed areas of the substrate will therefore be affected by plasma interactions than less exposed, more sheltered regions. Reproducibility and deposition control are often inhibited by these complex gas phase and surface dynamics. Other disadvantages include the creation of

undesirable compressive stresses particularly at lower frequencies and the generally more expensive and complicated nature of the equipment.

1.2.3.4.6 Applications of Plasma CVD: As mentioned above, the advantage of low deposition temperatures is particularly important for the fabrication of semiconductor materials due to the high possibility of interdiffusion at film thicknesses of about 2000 Å at high processing temperatures. For this reason semiconductor technology was the first major application for plasma CVD and remains its major application. Recently plasma has emerged as an application in deposition of films for cutting tools and wear and corrosion protection. The most important materials used in film products are the following[15,71,76-77]: a) silicon nitrides and silicon oxynitrides : Si_3N_4 films are used to completely passivate and encapsulate microelectronic devices because it is somewhat elastic and does not crack. Other benefits of this material is it provides an effective barrier against water and sodium and has good adhesion to aluminum and gold. However stoichiometry is difficult to control and hydrogen is often incorporated in the lattice structure where the material is then best described as $\text{Si}_x\text{N}_y\text{H}_z$. As much as 25% hydrogen can be incorporated into the film. While Si_3N_4 is denser, has higher resistivity and dielectric breakdown strength, and is more resistant to chemical attack, $\text{Si}_x\text{N}_y\text{H}_z$ can provide better step coverage. b) silicon dioxides: plasma-processed SiO_2 is used as an insulator in semiconductor devices and more recently as a coating for fiber optics. c) metals: PECVD has been used to synthesize transition metals, transition metal silicides and transition metal nitrides for the formation of conducting layers for barrier, contact, and

interconnect applications which will be described in more detail as it pertains to tungsten deposition. d) carbides and the elements carbon and boron have also been deposited using plasma CVD.

1.2.3.5 Photo-Enhanced Chemical Vapor Deposition (PHCVD): This type of process is based on activation of the reactants in the gas or vapor phase by electromagnetic (usually short wave ultraviolet) radiation[28,29]. Selective absorption of photonic energy by the reactant molecules or atoms initiates the process by forming very reactive free radical species that interact to form a desired film product. The advantages of this promising CVD process is the low temperature needed to form films and the greatly reduced radiation damage (compared to PECVD) that results. The limitations is the need for photoactivation with mercury to achieve acceptable rates of film deposition.

1.2.3.6 Laser-Enhanced Chemical Vapor Deposition (LCVD): Chemical vapor deposition involving the use of lasers can be categorized in two types of processes[30]: (1) pyrolysis (2) photolysis. In pyrolysis process the laser heats the substrate to decompose gases above it and enhance rates of chemical reactions there. Photolysis, on the other hand, involve direct dissociation of molecules by energetic photons. Among several advantages of these techniques are spatial resolution that can be achieved and the ability to interface with laser annealing, diffusion, and localized heat treatments, but LCVD is still in its early development.

1.3 Chemical Vapor Deposition of Tungsten

1.3.1 Tungsten Film Application

The semiconductor industry is experiencing rapid technological growth in the area of submicron IC device fabrication which has led to continually shrinking device feature size. Performance and reliability concerns for these approaches have led to consideration of low resistivity material, such as tungsten. In fact, tungsten applications at production level have already started. Tungsten provides low resistance ($5.6\mu\Omega\text{-cm}$ of bulk resistivity), low stress ($<5\times 10^9$ dyne/cm²), excellent conformal step coverage and a thermal expansion coefficient which is close to that of silicon. Another important feature for tungsten is its high resistance to electromigration, while in the current technology aluminum severely suffers from it [31].

There are two aspects of tungsten CVD for integrated circuits that have taken on commercial importance. One is the blanket deposition or nonselective deposition, in which deposition proceeds uniformly over variety of surfaces. A primary application of blanket W CVD is for interconnects, which is shown schematically in figure 1.3. Another application for blanket W CVD is via hole filling to planarize each level for subsequent processing. This is achieved by depositing a conformal film and etching back to the insulator surface (figure 1.3.). The second area of interest is the “selective” CVD of tungsten, where deposition occurs on silicon but not on silicon dioxide. Here one can selectively fill via holes to either provide a thin barrier metal or to deposit a thicker to help planarize the circuit. Both applications involve processing step, and are attractive for this reason [32].

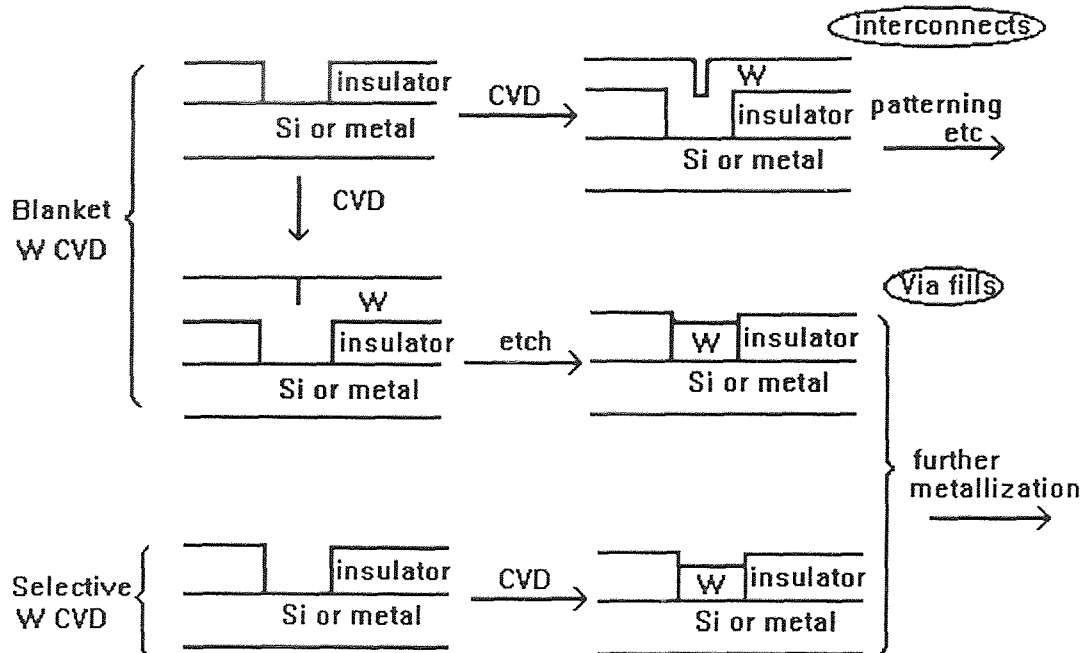


Figure 1.3 Schematic for applications of blanket and selective metal CVD for microelectronics applications

1.3.2 Reaction for CVD of Tungsten

Tungsten can be chemically vapor deposited by reduction of WF_6 or WCl_6 . The common reductant are silicon (Si), hydrogen (H_2), silane (SiH_4). Only a few studies were done on WCl_6 as the source of tungsten. Because W films deposited from WF_6 have an advantage over those deposited from WCl_6 in that lower contact resistance to Si may be achieved. Furthermore, WF_6 is a liquid that boils at room temperature, whereas WCl_6 is a solid that melts at $275^\circ C$, making its use as a CVD source more difficult[33]. Tungsten also can be deposited by the pyrolysis of $W(CO)_6$, the weaker W-CO bonds (CO is a neutral ligand)

allow for unimolecular dissociation at low temperature, but the deposition of W from $W(CO)_6$ does not exhibit selectivity [34].

The free energy change ΔG for WF_6 reaction at 600 K are given in Table 2 [35]. Comparing these free energies, the free energy of Si reduction is more negative than that of H_2 reduction. So when the H_2 reduction reaction is carried out, it is the Si substrate that first react with WF_6 . The substrate consumption will result encroachment, tunneling, creep-up and loss of selectivity problems[31]. After a certain W film thickness is reached this reaction will stop because the W film forms a diffusion barrier between the Si and WF_6 and prevents further reaction. This phenomenon is called self-limiting[36]. The SiH_4 reduction reaction is more favorable than the Si and H_2 reduction reactions. This reaction can suppress the Si reduction and Si consumption. Higher deposition rates at relatively lower temperatures and smoother resulting W/Si interfaces make this reaction very attractive. Recent developments of CVD tungsten have focused on this reaction.

1.3.2.1 Reduction WF_6 with Si: The reduction of WF_6 by solid silicon is of interest because of the potential of selective tungsten CVD for via hole filling for multilevel interconnect technology. This reaction is important because it is necessary to deposit some tungsten before the normal reduction processes, i.e., WF_6+H_2 or SiH_4 , can proceed. However, excessive consumption of silicon and other detrimental effects such as “wormhole” formation have limited the utility of this reaction.

Table 2 Free Energy Changes at 600 K

Reactions	ΔG , kcal/mol (based on 1 mole WF_6)
(A) $WF_6 + 1.5Si \rightarrow W + 1.5SiF_4$	-179.4
(B) $WF_6 + 3H_2 \rightarrow W + 6HF$	-27.9
(C) $WF_6 + 1.5 SiH_4 \rightarrow W + 1.5SiF_4 + 3H_2$	-208.7
(D) $WF_6 + 2.1SiH_4 \rightarrow 0.2W_5Si_3 + 1.5SiF_4 + 4.2H_2$	-227.6
(E) $WF_6 + 3.5SiH_4 \rightarrow WSi_2 + 1.5SiF_4 + 7H_2$	-268.9

Fortunately, from a processing point of view, the Si + WF_6 reaction has often been found to be “self-limiting” and typically only 100 to 200Å of tungsten is deposited. The reaction is also very fast and reaches the self-limited thickness in a few seconds at typical LPCVD conditions. For the results of Broadbent and coworkers [37] the self-limiting thickness is deposited in 6 s and no additional deposition occurs for the time up to 6000s. Despite a lot of effort, the mechanism leading to self-limiting deposition is still not completely understood. One theory is that once a continuous tungsten film is formed the reaction slows down dramatically or shuts off completely because it becomes limited by transport of one of the reactants to the active interface. One difficulty with this idea is that some self-limiting films appear to be very porous, although others have near bulk tungsten densities. Another theory [38] is that a “blocking” agent, namely, WF_4 , builds up on the tungsten surface and inhibits deposition.

Green, et al.[39] examined the morphology of Si-reduced W films deposited between 210 and 700°C. The grains were spongy in structure, and the space is occupied by trapped gases and pores. Therefore, the film density was far less than tungsten bulk density.

Auger depth analysis showed that most of the oxygen in the W film is present at the Si/W interface[40]. Joshi,et al. [41] found 22-25% oxygen in the films deposited below 600°C, causing high film resistivities (130-140 $\mu\Omega\text{-cm}$). The oxygen level drops to 12-14% at higher temperatures resulting in lower resistivities (60-70 $\mu\Omega\text{-cm}$). A native oxide layer on the silicon surface was reported to be incorporated into the W films[42].

1.3.2.2 Reduction WF_6 with H_2 : It was found that the H_2+WF_6 CVD process could be selective in that deposition occurred rapidly on many metals and semiconductors, but not on insulators such as SiO_2 . Selectivity apparently occurs because deposition requires that the substrate be capable of either reducing WF_6 to metallic W, or dissociatively chemisorbing H_2 and WF_6 . Most oxides do not readily support either of these processes and therefore tungsten deposition does not readily occur. The selective nature of the deposition process created much interest in that it significantly reduced the number of steps in the metallization process.

There have been numerous experimental kinetic studies covering LPCVD and APCVD conditions over a wide temperature range. Creighton, et al. [32] categorized them into two regimes. The first reaction regime described as being dominated by homogeneous reactions obeyed the following pressure dependence

$$\text{Rate} \propto P(\text{WF}_6)^2 \cdot P(\text{H}_2)^2 \quad (1.6)$$

The conditions that lead to this kinetic regime generally have not been studied further. In another regime the reaction proceeded heterogeneously with the following pressure dependence

$$\text{Rate} \propto P(\text{WF}_6)^0 \cdot P(\text{H}_2)^{1/2} \quad (1.7)$$

and an apparent activation energy of ~66.24 kJ/mol. The form of the rate law above has been verified by numerous workers for LPCVD conditions[43,44]. The phenomenon that the deposition rate depends on the H₂ flow rate, not on WF₆ rate suggests that surface-adsorbed H₂ dissociation is the rate-controlled mechanism.

Selective deposition of W on Si surfaces constitutes another area of concern in the H₂-reduction reaction. Joshi, et al. [45] have found that the selectivity of tungsten produced by silicon reduction is almost 100% while that by H₂ reduction depends on the prior condition of the Si wafer. McConica and Krishnamani [43] observed that the selectivity loss to silicon surfaces occurs at temperature higher than 300°C. The temperature dependence suggested that the tungsten nucleation on the oxide is an activated process. In an ultra high vacuum (UHV) analysis chamber, Creighton[46] performed Auger electron spectroscopy and temperature programmed desorption studies on the selectivity loss. He suggested that a tungsten subfluoride desorption-

disproportionation mechanism is the origin of transport of tungsten from the tungsten surface to the silicon dioxide surface. Tungsten pentafluoride, WF_5 , was the best candidate to initiate the selectivity loss because of its volatility.

Studies of the CVD tungsten film morphology and impurity content are essential for the film quality, and thereby the film resistivity. Shroff and Delval [47] have measured the fluorine content of W films with photon activation analysis. The deposition of low fluorine content films was possible at high temperature, high H_2/WF_6 ratios and low pressures. Initial tungsten layers always started with a fine grain structure on the base metal substrates and continued to grow as elongated crystals. It was also reported that increasing H_2/WF_6 ratios and higher pressures resulted in less adherent and inhomogeneous coatings. This was exacerbated at high temperature due to nucleation in the vapor phase.

R.A.Levy[48], et al. observed wormhole formation in the Si substrate. They also reported that the wormhole is non-crystal resulting from both Si and H_2 reduction of WF_6 . McLaury[49], et al. have found that fluorine was a major contaminant in the films. Transmission electron microscopy studies revealed damage at the (100) Si/SiO₂ interface in the form of worm tracks. Stacy[50], et al. performed TEM analyses on the W films and confirmed tungsten deposition filaments (also called wormholes or tunnels) in the silicon substrate. Joshi[45], et al stated that H_2 reduction produces purer films than Si reduction by getting oxygen in the reaction chamber. Thus, the resistivities for H_2 reduced films (9-10 $\mu\Omega$ -cm) are far less than those of Si reduced films (130-140 $\mu\Omega$ -cm). They also noted that hydrogen reduction produces very rough films compared to silicon reduction.

The frequently observed preferential tungsten crystal orientation in the H_2 reduction reaction is W(100)[47]. High H_2/WF_6 ratios have been reported to give W(111) orientation[51]. In a more detailed structural study, Kamins[52], et al. examined orientation change with thickness for W films. They used a chromium nucleation layer to prevent the Si- WF_6 reaction from influencing the W film structure.

R.V.Joshi[53] found W film stress deposited from H_2 reduction is a strong function of temperature and a weak function of H_2/WF_6 ratio and pressure. High temperature, pressure, and H_2/WF_6 favor lower W film stress. The higher temperature, the lower stress. Other researchers[54] reported similar trend of stress dependency on temperature and H_2/WF_6 ratio and found the tensile to compressive stress conversion at chuck temperature of 500-700°C for a pressure of 1.5 Torr.

1.3.2.3 Reduction WF_6 with SiH_4 : In addition to H_2 the reduction of WF_6 may be accomplished by a number of reducing gases and the most important alternative to H_2 is silane (SiH_4). SiH_4 is known to readily dissociatively chemisorb on clean tungsten surfaces. This tungsten CVD process via silane reduction is similar to the tungsten silicide CVD process that uses higher SiH_4/WF_6 pressure ratios and usually deposits in a nonselectively fashion[55]. For low SiH_4/WF_6 ratios (typically less than 1:1) the process leads to α -W deposition, often with a high degree of selectivity. At somewhat higher SiH_4/WF_6 ratios (typically 1 to 3) the process leads to higher resistivity deposits of β -W or tungsten silicides, usually in a nonselective fashion. Some of the original work using silane as a reductant was actually aimed at preventing excess silicon substrate

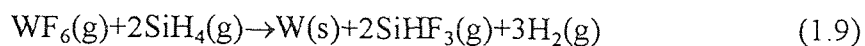
consumption or other detrimental interactions of WF_6 (+ H_2) with the substrate such as encroachment or “wormhole” formation. In addition to the demonstrated selectivity and minimized silicon substrate damage, the process also generated interest because of the extremely high growth rates that could be achieved at relatively low temperature (up to $\sim 1\mu\text{m}/\text{min}$ at 300°C). Some of the original enthusiasm has dampened as many workers found selectively difficult to maintain on a reliable basis, as was the case with the hydrogen reduction process.

Most of the kinetic studies [56] of the silane reduction process have been performed in LPCVD reactors. A weaker temperature dependence and the pressure dependence are generally observed:

$$\text{Rate} \propto P(WF_6)^n P(SiH_4)^1, \text{ n typically } \sim 0 \text{ or slightly negative} \quad (1.8)$$

The higher deposition rates and weak temperature dependence led a number of workers to suspect that the deposition process was mass transport limited.

Kobayashi[57], et al. used *in situ* infrared spectroscopy to sample the gas phase above a wafer in an LPCVD reactor during deposition. They found no evidence for HF production at typical CVD temperatures (250 to 350°C) but found that $SiHF_3$ rather than SiF_4 was the main silicon fluoride produced, so they proposed the possible reaction pathway as follows:



The resistivity of tungsten deposited from silane reduction is related to the impurity content. Juugd[58], et al. employed AES and electron probe micro analysis to elucidate resistivity dependence on the incorporated silicon. On the contrary, Suzuki[59], et al. stated that resistivity depends mostly on fluorine content, as determined by SIMS analysis, rather than silicon and oxygen content. The film from SiH_4 reduction has higher resistivity value than that from H_2 . S.Sivaram[60], et al. found not only the impurity content but also the microstructure account for this difference.

Orientation of deposited films is another factor to be considered for kinetic evaluations. X-ray diffraction patterns in some research papers showed a (110) preferred orientation of tungsten crystals when α -W was the dominant phase[35,55,59]. In contradiction to these, Schmitz[61], et al. reported a dominant (100) orientation for both H_2 - WF_6 and SiH_4 - WF_6 systems. These distinction may be a result of different deposition kinetics and/or be the different substrates.

The film deposited from silane reduction has higher stress than that from H_2 reduction[62]. Takayuki[63], et al. found different types of heating lead to different stress in the W film deposited from SiH_4 reduction. In IR-heating from the wafer back and in resistance heating, stress is tensile stress at low deposition temperature. The tensile stress decreases as deposition temperature increases. In IR-heating from the wafer front, stress is compressive at all deposition temperature. Takashi[64], et al. use ECR plasma CVD system to deposit W film which has a low compressive stress due to ion bombardment.

1.3.2.4 Dissociation of $W(CO)_6$: Tungsten hexacarbonyl, $W(CO)_6$, is a stable solid with a relatively low vapor pressure (350 mTorr at 500 °C). Because the W-CO bond energy is relatively weak (~43 kcal/mol) compared with the W-F bond energy (~121 kcal/mol). This allows for tungsten deposition at relatively low temperatures without the aid of a reducing agent. Factors that have limited the utility of $W(CO)_6$ are the inconvenience of using a solid source, its low vapor pressure, and the incorporation of carbon and oxygen into the deposits.

Relatively clean α -W can be deposited above 450°C at a rate of ~100Å/min and with resistivities 3 to 6 times the bulk value. Films deposited below 450°C are normally heavily contaminated with carbon, resulting in resistivities 20-300 times the bulk value, and exhibit an fcc crystal structure. The deposition rate exhibited an apparent activation energy of 18 kcal/mol[32].

Tungsten deposition via $W(CO)_6$ decomposition is nonselective toward Si and SiO_2 . Films deposited on silicon oxides are generally adherent, in contrast to the hydrogen reduced WF_6 films. The hexacarbonyl process does not produce the deleterious effects at the silicon interface that are sometimes seen with the hexafluoride processes. This is not surprising because CO interactions with silicon are rather weak and do not lead to gas phase products.

1.4 Plasma Enhanced Chemical Vapor Deposition of Tungsten Films

1.4.1 PECVD Tungsten Film Overview: There has been little work reported on plasma-enhanced CVD of tungsten as compared to LPCVD, however PECVD of other conducting

films of refractory metals such as tungsten silicide, molybdenum and its silicide, and titanium and tantalum silicides have been carried out [77-79]. These transition metal films require a volatile source of the transition metal, such as halides, carbonyls, and alkyls as the reactant source. The highly reactive atmosphere of PECVD results in inclusion of halogen, carbon, and oxygen into the growing films. The primary effect of these inclusions is an increase in resistivity of the as-deposited films [77]. In addition, halogen atoms generated by the plasma serve as an etchant species for the depositing film. Tungsten is an example in which a conventional RF (4.5 MHz) plasma-enhanced CVD technique had been applied to the low temperature deposition of tungsten film in a pure WF_6 discharge. The resulting films were porous at temperatures below $90^\circ C$ were porous due to the high concentration of reactive fluorine generated in the plasma discharge. At higher temperatures, no deposition occurred as a result of fluorine etching, attributable to the high concentration of fluorine atoms generated in the plasma atmosphere from electron impact dissociation and ionization of WF_6 . However, the addition of hydrogen to the WF_6 plasma resulted in fluorine atom scavenging and the prevention of tungsten etching at temperatures as high as $400^\circ C$. Removal of the oxide substrate due to fluorine etching can be eliminated by larger flows of hydrogen for a complete neutralization of the generated fluorine atoms [36]. Dilution effects decrease the growth rate with increasing hydrogen additions, however, increasing deposition temperatures favor the formation of the lower resistivity α -phase tungsten, which will be discussed later in the section on resistivity of PECVD tungsten film. A lower discharge frequency (100 kHz) WF_6/H_2 process has been used to deposit tungsten at enhanced deposition rates with an activation energy (0.23 eV) three

times less than that of LPCVD[36]. The use of a microwave discharge is a method for clean electrodeless plasma generation. For conductive films, the use of ECR plasma CVD for conductive film deposition is difficult due to the difficulty in maintaining a continuous ECR plasma discharge. Microwaves are reflected or absorbed by the conductive films deposited on the microwave window. To combat this, Akahori et al[64] developed an ECR plasma process in which an RF bias was applied to the window and Ar gas was introduced into the plasma reaction chamber during deposition. This resulted in conductive film deposited on the window to be sputtered and removed. The ECR discharge could then be maintained, with an unchanged deposition rate even after a long time. As a result of the additional plasma activation process of the high density, low pressure microwave process in which the ion bombardment flux is significant with respect to the flux of reactive species the purity, structure, stress, surface morphology and resistivity of W films can be improved by the effect of the ion bombardment[81-82].

1.4.2 Reaction of PECVD For Tungsten: Plasma deposition reactions permit an increase in the deposition rate without an increase in temperature. However the complex gas phase with the large variety of reactive species that may be present and the surface chemistry make the kinetics and reaction mechanisms difficult to understand.

1.4.2.1 PECVD Reduction of WF_6 with H_2 : The chemical vapor deposition of tungsten from its hexafluoride takes place via silicon- or hydrogen- reduction reactions as described above with the LPCVD process (equations A) and B) respectively, Table 2)

with equation 1.7 describing the reaction rate for the observed reaction kinetics due to the hydrogen reduction of WF_6 on the growing surface. Plasma-enhanced CVD of tungsten onto silicon is heterogeneous as shown by a strong pressure dependence with little or no flow rate dependence[80]. The deposition rate dependencies on the partial pressures of H_2 and WF_6 at constant temperatures indicate a linear dependence on WF_6 partial pressure and a much weaker dependence on H_2 partial pressure, possibly half-order. The deposition rate reaction kinetics can be given by the following equation:

$$\text{Rate} = K_p [WF_6]^1 p[H_2]^{1/2} \text{Exp}(-0.16\text{eV}/kT) \quad (1.10)$$

in units of $\mu\text{g cm}^{-2} \text{min}^{-1}$ with an activation energy $0.16 \pm 0.03 \text{ eV/atom}$ [77,80]. Both the activation energy and reaction kinetics differ markedly from LPCVD, suggesting a different rate limiting step. The activation energy of the hydrogen-reduction reaction in LPCVD, .7 eV/atom, associated with the rate limiting step of the reaction, is believed to be the dissociative adsorption of hydrogen on the substrate surface or desorption of the by-product HF. However in a glow discharge, monatomic hydrogen is created by electron impact dissociation in the gas phase or ion bombardment induced dissociation of H_2 on the surface. Hydrogen is then available for reaction with WF_x species so the thermal dissociation of hydrogen is not important and is not the rate-determining step. It is believed that the silicon- and hydrogen-reduction reactions are proceeding simultaneously, with the silicon-reduction mechanism dominating. This is evidenced by one study[82] by the deposition of thin, porous, polycrystalline films similar to those observed in silicon-

reduction reaction LPCVD tungsten films. The much reduced hydrogen dependence suggests a much lower rate of any hydrogen-reduction deposition. On tungsten and GaAs substrates, however, there was a first-order dependence on hydrogen partial pressure with hydrogen reduction of WF_6 the deposition mechanism. The reaction between silicon and tungsten (equation A), Table 2) has a large free energy and is not expected to be the rate limiting step, since the much slower hydrogen-reduction reaction is not limited by the rate of tungsten adsorption. The rate-limiting step is believed to be the diffusion of tungsten fluoride molecules from the surface through the film, aided by the polycrystalline and porous nature of the films that contain many voids between the crystal grains that enhance the diffusion process.

CHAPTER 2

THE DEPOSITION PROCESS OF TUNGSTEN FILM

2.1 Reaction System

2.1.1 Equipment Set up

The deposition reaction was carried out in a SPECTRUM model 211, cold wall, single wafer CVD tungsten reactor system fully automated computer control as shown in figure 2.1. In this system 10 cm diameter silicon wafers are loaded through a load-lock by a cassette-to-cassette transport facility. The wafer is positioned against the quartz window in an inverted position and held in place by a lift pins, which leaves the front side exposed to the reactant gases. The wafers are heated on the backside by means of radiant energy through the quartz window, which was generated from a quartz lamp.

The gases used for the experiments are semiconductor-grade tungsten hexafluoride (WF_6) and semiconductor-purity hydrogen (H_2). The WF_6 was provided in an stainless steel container, which was attached to the reactor through a adjust valve. The hydrogen was directly connected with the chamber. The gas flow rate was controlled by the Gas Controller Module in the Spectrum 211. The controllable operation range for mass flow controller are 0-10 sccm (standard cubic centimeters per minute) for tungsten hexafluoride and 0-1000sccm for hydrogen.

Two vacuum pump packages are used in this system. The pump package is a pump system which combined one booster and one rotary vane pump. One pump

pressure at the set point. The second pump package was used to transport the wafer to the chamber. Additional rotary vane pump is used to pump the WF_6 to the air during the ramp and temperature stabilize steps. At these two steps, WF_6 valve is opened to keep the WF_6 flow rate stable.

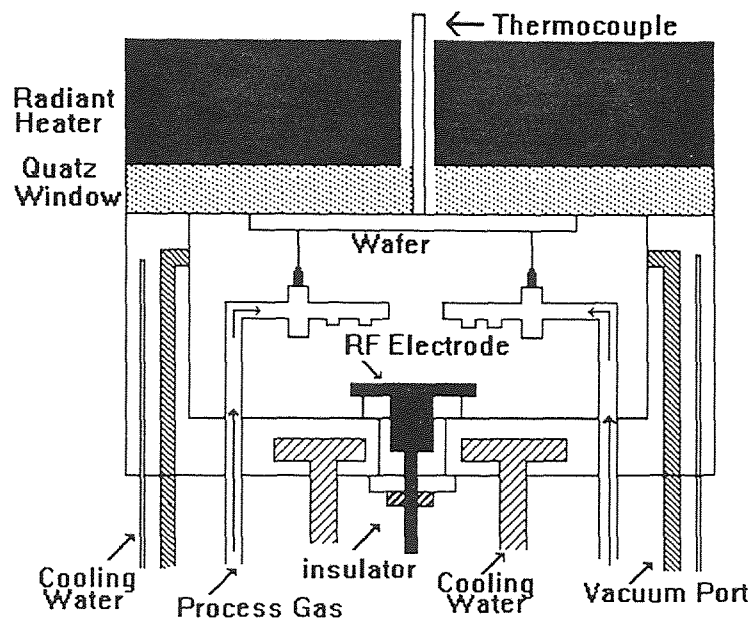


Figure 2.1 Schematic diagram of the chamber

2.1.2 Pre-deposition Preparation

2.1.2.1 Leak Check: A leak check was conducted before beginning of any experimental run to avoid oxygen and ensure formation of films with desirable and reproducible quality. For the SPECTRUM CVD 211, all experimental conditions can be directly read from the monitor; therefore, during this leak check procedure, the chamber was

connected to a vacuum system, the pressure decreased to near zero. This process takes several seconds.

2.2 Experimental Procedure

2.2.1 Wafer Preparation and Transport

All wafers were marked first, and weighed accurately to 0.1 mg before and after deposition. In this system 10 cm diameter single crystal, <100> silicon wafers are loaded through a load-lock by a cassette-to-cassette transport facility. The whole wafer transport was carried out by automatic control of the machine, and the whole operation process also can be controlled from the monitor.

2.2.2 Film Deposition

The film deposition is achieved in five steps process: (1) pre-purge, (2) ramp up (increasing the reactor temperature rapidly from room temperature to set point), (3) temperature stabilize (time: 30 seconds), (4) tungsten deposition, (5) post purge. The purposes of pre-purge and post-purge are cleaning the chamber. They are divided into several substeps (Table 2). During the ramp and temperature stabilize steps, H_2 is introduced into the chamber and the WF_6 is directly connected with a separate vacuum pump which pumps the WF_6 to the air. In the deposition step, WF_6 is switched to the chamber. The reactor wall were maintained at $30^\circ C$ by using cooling water at that temperature. During deposition the flow rate, the temperature and the reactor pressure was kept in a small range around the set point.

Table 2 The detailed sub-step in the Pre-purge and Post-purge step

Pre-purge		post-purge	
sub-step	condition	sub-step	condition
1)Purge	P>30mTorr	(1) Pump own	P<10mTorr
2)Pump down	P<10mTorr	(2) Pump own	T=30 second
3)Pump down	T=10 second	(3) Purge	P>30mTorr
4) Purge	P>30 mTorr	(4) Pump down	P<10mTorr
5)Pump down	P<10 mTorr	(5) Pump down	T=30 second
6)Pump down	T=10 second	(6)Purge	P>30 mTorr
		(7) Pump down	P<10mTorr
		(8) Pump down	T=30 second
		(9) Purge	P>30mTorr
		(10)Pump down	P<10mTorr
		(11)Pump down	T=30 second
		(12)Purge	P>30mTorr
		(13)Pump down	P<10mTorr
		(14)Pump down	P>30mTorr

2.3 Tungsten Film Characterization Techniques

2.3.1 Physical Property

2.3.1.1 Film Thickness: The weight change of the wafer after the deposition was measured by electrobalance. Known the wafer area A (78.54 cm^2), and the mass change after deposition, Δm , tungsten film thickness, t , is found from the formula:

$$t = \frac{\Delta m}{\rho_b A} \quad (2.1)$$

A constant bulk density, ρ_b , of 19.3 g/cm^3 [65] is assumed throughout the calculations.

2.3.2 Structure Property

2.3.2.1 X-ray Diffraction Analysis: The crystallographic orientation of the CVD tungsten film was established by X-ray diffraction measurements using with a Cu target on a Rigaku DMAX II system operating at 30KV and 20mA. Scanning speed of the Goniometer is $2^\circ 2\theta/\text{min}$. Tungsten deposited Si wafers are scanned through a 2θ range of $20\text{-}90^\circ$.

2.3.3 Electrical Property

The sheet resistance values are directly measured by a home-built 4-point probe equipment. The probes are placed colinearly, as shown in figure 2.2 [66]. In this configuration, a constant current I is passed through two of the probes, and the voltage difference between the other two is read. Provided the conducting layer is thin, the sheet resistance can be calculated from the equation

$$R_s = \frac{\pi}{\ln 2} \frac{V}{I} \quad (2.2)$$

In this experiment, sheet resistivity is measured at different locations on each wafer as shown in figure 2.3. The ranges of voltage and current used in measurements are 1-10 mV and <100 mA, respectively. All the measurements are taken at room temperature.

The film resistivity can be calculated using the resistance. Consider a rectangle of a layer of length l , width b , and thickness t as shown in figure 2.2. The resistance measured in the direction parallel to the film is

$$R_s = \rho \frac{l}{bt} \quad (2.3)$$

where, ρ is the resistivity of the film. If l equal to b , the equation shown as above becomes

$$R_s = \frac{\rho}{t} \quad (2.4)$$

when the thickness and sheet resistance are measured, the film resistivity can be calculated by

$$\rho = R_s t \quad (2.5)$$

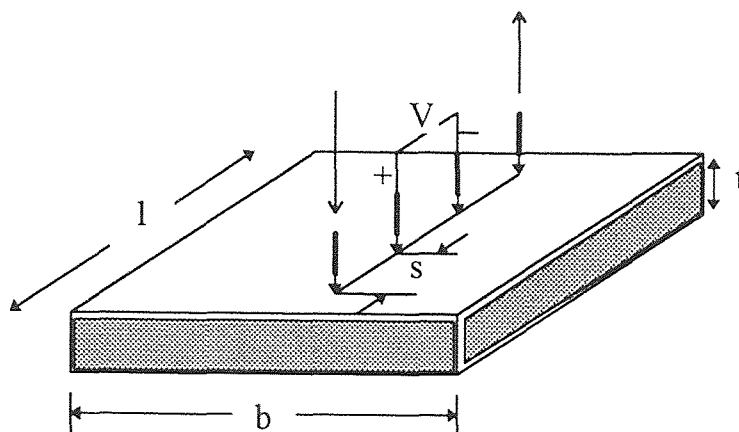


Figure 2.2 Four-point probe system for sheet resistance measurement.

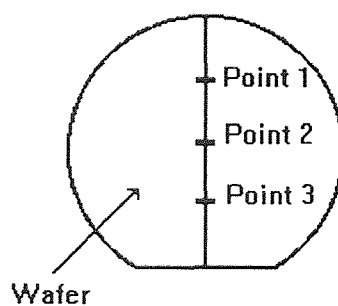


Figure 2.3 The resistivity measurement position on the wafer

2.3.4 Mechanical Property

Film Stress was determined by measuring changes in the radius of curvature of a wafer resulting from deposition on a single side. The distance between two points generated by light from two fixed and parallel He-Ne lasers was determined by reflection from the surface of a wafer before and after deposition. An angled mirror was used to project the

reflection of the two points onto a wall where their separation could be accurately measures. The stress was calculated using Stoney's equation [67]:

$$\sigma = Et_s^2 / 6(1-\nu)Rt \quad (2.6)$$

where E is Young's modulus for the substrate, ν is Poisson's ratio, t_s is the substrate thickness, t is the film thickness, and the net radius of curvature is

$$R = 1 / (1/R_2 - 1/R_1) \quad (2.7)$$

where R_1 and R_2 are the radii of curvature of the wafer before and after deposition

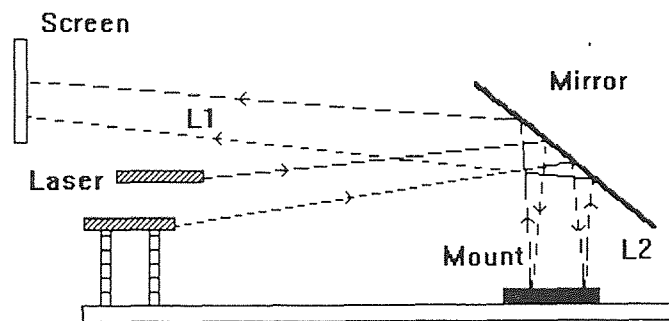


Figure 2.4 Optical system for stress measurement setup

respectively. For Si <100> wafers, $E = 1.8 \times 10^{11}$ Pa and $t_s = 525$ μm . Figure 2.4 shows an optical imaging system for set up.

CHAPTER 3

RESULTS AND DISCUSSION

3.1 The Effects of Deposition Variables on Film Deposition Rate

3.1.1 Temperature Dependent Study

The temperature dependent behavior of deposition rate is shown in Figure 3.1 for the conditions of a constant WF_6 flow rate (5 sccm), H_2 flow rate (100 sccm) and the total reactor pressure (500 mTorr). The figure shows a typical deposition rate vs. temperature dependency for this type of deposition reaction. Two different regimes can be seen which are defined by the rate limiting mechanism of the reaction: (1) The first regime is from 300 °C to 600 °C, the growth rate of tungsten increase quickly with temperature. This regime is controlled by the surface reaction rate.(2) The second regime is above 600 °C. The growth rate of tungsten increase slightly with temperature. This regime is controlled by the rate at which reactant is supplied to the substrate. The reaction rate controlled regime seems to follow an Arrhenius type behavior. An activation energy of about 56 kJ/mol was calculated from the slope in the region where Arrhenius behavior was observed (300-500 °C) by using a linear regression analysis to the following equation:

$$\text{Growth Rate} = k_0 \times e^{\frac{-E_a}{R \cdot T}} \quad (3.1)$$

This result is comparable to the value 69 kJ/mol reported by Mcconica [43]

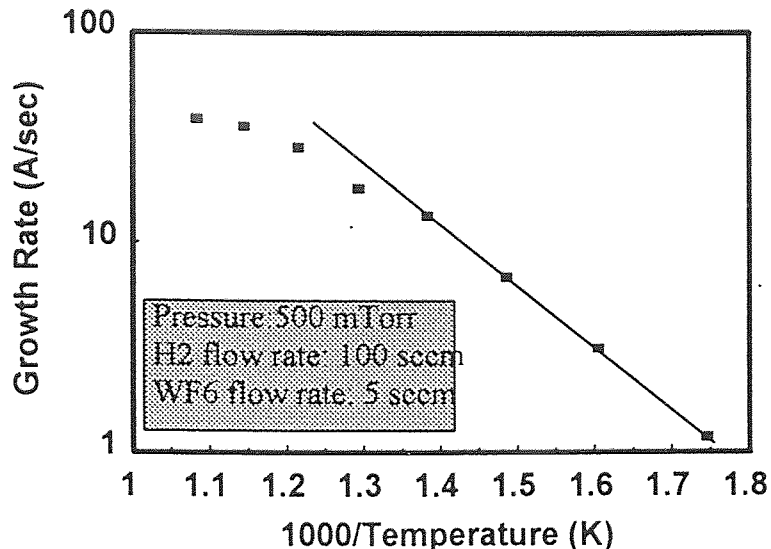


Figure 3.1 Variation of growth rate as a function of temperature at a constant total pressure, WF_6 flow rate, and H_2/WF_6 ratio

3.1.2 Pressure Dependent Study

Under constant conditions of temperature ($500\text{ }^\circ\text{C}$), WF_6 flow rate (5 sccm), and H_2/WF_6 ratio (20/1), the pressure dependent behavior of growth rate dependence on pressure was investigated over the range 100 to 1000 mTorr. The results, shown in Figure.3.2, indicate a linear dependence which is consistent with a Langmuir-Hinshelwood mechanism. The higher the pressure, the more gaseous adsorbed reactants on the substrate surface, the faster the growth rate. The linear line does not have a zero-pressure intercept caused by the fast Si reduction of WF_6 . To obtain the relationship of H_2 partial pressure with the growth rate, first we assume the equilibrium condition to calculate the H_2 partial pressure in the chamber. The quantity of all the species in the chamber are defined as:



$$F_{H_2}-3X \quad F_{WF_6}-X \quad X \quad 6X \quad (3.3)$$

F_{H_2} and F_{WF_6} are the flow rate of H_2 and WF_6 respectively. X is the quantity of WF_6 which is converted to W . Because the reactor was cold wall type and the W selectively deposited on the Si wafer not on the quartz window, we assume all the W are deposited on the Si wafer. So we can use the W growth rate R (cm/sec) and the Si wafer area to calculate X (sccm):

$$X=R \times S_{\text{wafer}} \times \rho / M \times 22400 \times 60 \quad (3.4)$$

S_{wafer} is the area of the wafer, which is 78.54 cm^2 . ρ is the tungsten density, which is 19.3 g/cm^3 . M is the molar weight of tungsten, which is 183.85 g/mol . After calculating the X , the partial pressure of H_2 can be easily calculated:

$$P_{H_2} = \frac{F_{H_2} - 3X}{(F_{H_2} - 3X) + (F_{WF_6} - X) + X + 6X} \times P_{\text{total}} \quad (3.5)$$

The relationship of H_2 partial pressure with growth rate is shown in figure 3.3. The diagram shows a linear dependence which is different from other reporter[43,44]. This may be due to the different reactor and different pressure range. Such linear dependence is consistent with a Langmuir-Hinshelwood reaction mechanism. Mcconiica, et al [43]

point out the adsorption of hydrogen is growth rate limited step,. So according to the Langmuir-Hinshelwood mechanism, the growth rate of tungsten for low pressure deposition is given as:

$$\text{Rate} = kKP_{\text{H}_2} / (1 + KP_{\text{H}_2}) \quad (3.6)$$

Where k is the reaction rate constant and K is the adsorption equilibrium constant. For low pressure values, KP_{H_2} is small compared to 1 thus yielding the observed linear dependence.

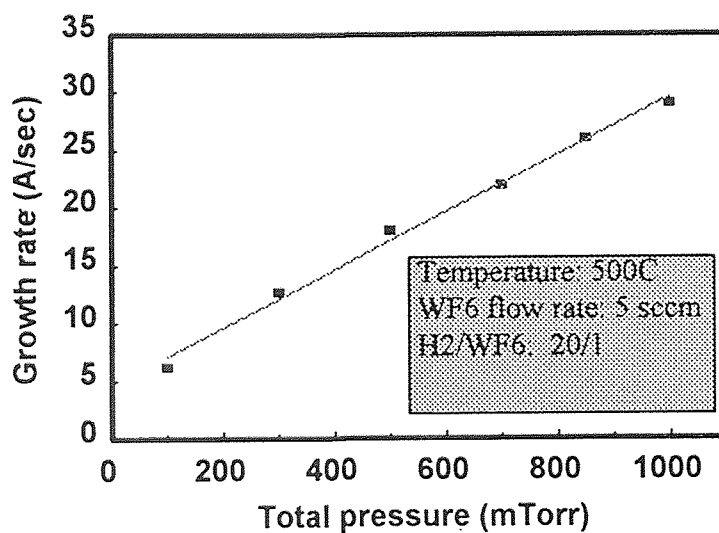


Figure 3.2 Variation of growth rate as a function of total pressure at a constant temperature, WF_6 flow rate, and H_2/WF_6 ratio

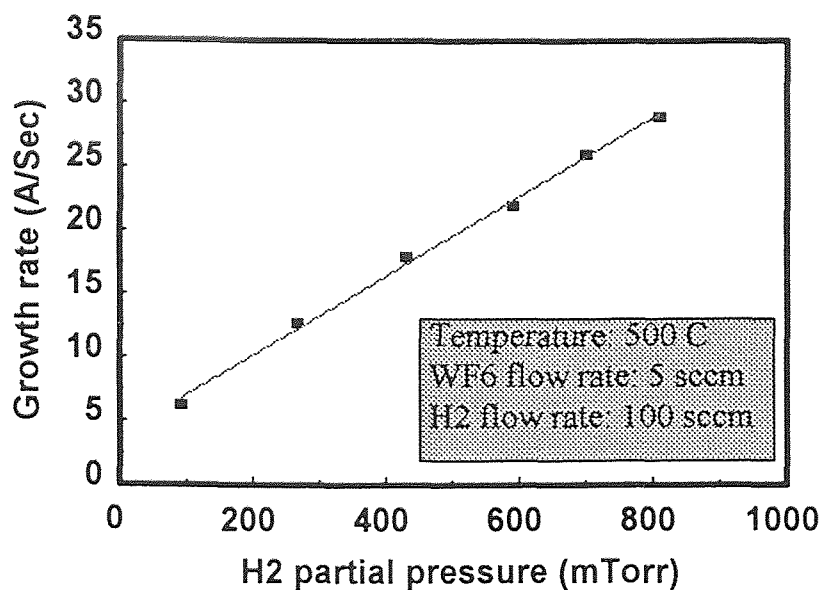


Figure 3.3 Variation of growth rate as a function of H₂ partial pressure at a constant temperature and WF₆ flow rate, and H₂/WF₆ ratio

3.1.3 Flow Ratio Dependent Study

In Figure.3.4, the deposition rate is plotted as a function of H₂/WF₆ ratio for constant conditions of growth temperature (500°C), total pressure (500mTorr) and WF₆ flow rate (5sccm). The deposition rate was found to increase in the low flow ratio regime (below 10) followed by saturation above this flow ratio. The former H₂ partial pressure effect on growth rate study show that the deposition rate increase with the partial pressure of H₂. Therefore, when the flow ratio (H₂/WF₆) increase, the partial pressure of H₂ increase, the deposition rate increase. But after the flow ratio reach a certain value, the H₂ in the chamber will saturate and not enough WF₆ is present to meet the increasement of deposition rate. The deposition rate will no longer increase.

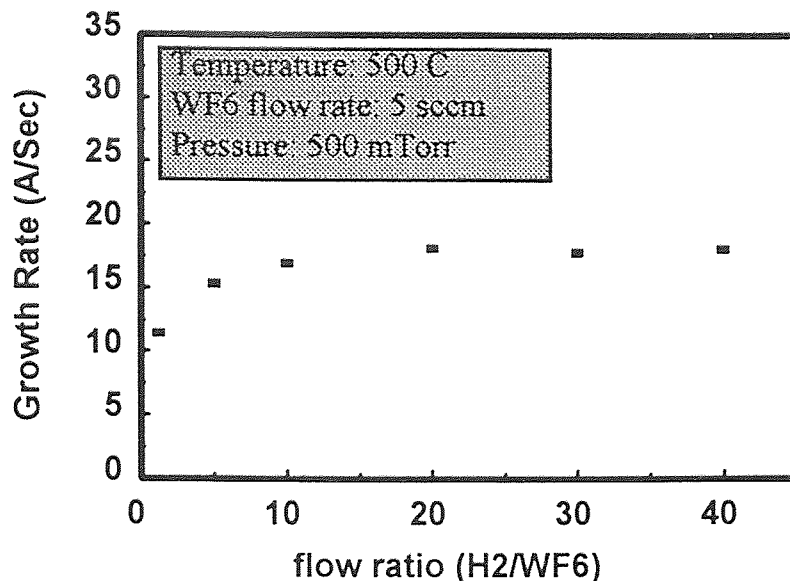


Figure 3.4 Variation of growth rate as a function of flow ratio at a constant temperature, pressure and WF₆ flow rate

3.2 Tungsten Film Characteristics

3.2.1 Stress

The stress of the deposited film is a very important aspect of tungsten film for X-ray absorber application and as interconnect material. Stress in the absorber exerts a torque on the membrane at the edges of features, and this leads to out-of-plane and in plane distortion. In order to find the effect of deposition condition on film stress, three operation parameters are considered to be variables for the stress studies. The three studies are based on the standard reaction condition (growth temperature 500°C, total pressure 500 mTorr, the flow ratio of H₂ to WF₆ 20). The ranges for these parameters were varied from 300-625°C for the temperature series, from 100 to 1000 mTorr for

pressure series and from 1 to 40 for flow ratio series. These results are shown in Figure 3.5, 3.6 and 3.7 respectively.

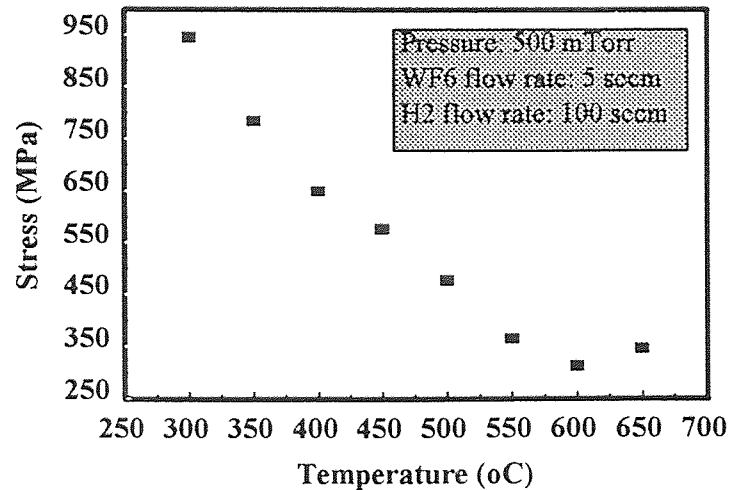


Figure 3.5 Variation of stress as a function of temperature at a constant pressure, WF_6 flow rate, and H_2/WF_6 ratio.

3.2.1.1 Temperature Effect: It is clear the stress in the tungsten film has a strong relationship with temperature. Between the 300 and 600°C, the stress decrease largely with temperature. According to the buried layer (BL) model for steady-state film growth proposed by Klokholm and Berry[68], it is suggested that tensile growth stresses are generated “ by the annealing and constrained shrinkage of disordered material buried behind the advancing surface of the growing film.” It is assumed that the amount of built-in disorder is proportional to the final stress in the film after complete relaxation. The model predicts that the tensile growth stress increases with increasing growth rates and/or decreasing deposition temperatures.

The measured tensile growth stress at approximately 7000Å thickness can be analyzed using the concepts of Klokholm and Berry. An activated surface relaxation process is defined with atomic jump frequency ν :

$$\nu = \nu_0 \exp(-E_s/RT) \quad (3.7)$$

with ν_0 a frequency factor, E_s an activation energy, R the gas constant, and T the absolute substrate temperature. The number of jumps n_j a surface atom can make before it is buried behind the growing surface will then approximately be

$$n_j \approx \nu r^{-1} \quad (3.8)$$

with r the growth rate in monolayers (ml) per second. If this number of jumps is low, lattice defects will be present in an as-deposited incremental layer of the film. These defects represent an excess volume ΔV_m , which, due to relaxation, will be transformed to an elastic strain in the film. The excess volume is defined as the difference between the molar volume of the as deposited, unrelaxed film and the molar volume V_m of a relaxed constrained film. If we assume this excess volume to be proportional to n_j^{-1} , then

$$\frac{1}{3} \frac{\Delta V_m}{V_m} = \varepsilon = \sigma \frac{1 - \nu_f}{E_f} = k n_j^{-1} = k r \nu^{-1} \quad (3.9)$$

or

$$\ln \frac{\varepsilon}{r} = \ln \frac{k}{v_o} + \frac{E_s}{RT} \quad (3.10)$$

where ε is the biaxial strain, σ is the biaxial stress, and k is a proportionality factor. Assuming the tungsten film's modulus ($E_f = 410$ GPa) is not dependent on the deposition temperature and is almost elastically isotropic ($\nu_f = 0.28$), so 1 GPa biaxial stress corresponds to 0.18% biaxial strain. According to Equation 9 the strain increases linearly with the growth rate, while it decreases exponentially with the deposition temperature. If the above mentioned model is valid, the logarithm of εr^{-1} , as determined from the σ values, versus the reciprocal absolute temperature should yield a straight line. Taking the thickness of a W monolayer, 2.74 Å, a straight line is obtained, with a slope corresponding to 59 kJ/mol. This value is different from the value 143 kJ/mol reported by Leusink et al. [69].

After temperature is higher than 600°C, stress increase slightly. This may be due to the strong substrate encroachment. The higher the temperature, the more the silicon consumption problem. Kamins, et al. [70] concluded that a significant contribution to the stress can arise from the initial reaction between the WF_6 and Si and little intrinsic stress is added during the hydrogen reduction reaction. The high substrate encroachment lead to the higher stress. Another Reason is that the reaction is in the mass-transport limited regime, the film always has sufficient time to complete relaxation before buried by the advancing surface of the growing film. So the stress no longer has relationship with the

temperature. This suggests E_s in the buried layer model is only applicable in the reaction rate limited regime.

3.2.1.2 Effect of PECVD on Stress: For the PECVD process, the temperature effect on stress was evaluated (figure 3.7) For the temperature range 400 -600 °C, the parameter constants were the following: RF plasma power 50 W, reactor pressure 200 mTorr, and WF_6/H_2 flow rate ratio of 100 sccm/5 sccm = 20 with the reactor wall temperature approximately room temperature. The decreasing stress with increasing temperature is consistent with the trend observed with LPCVD tungsten deposition. Similarly, Wong and Saraswat[83] found that post-deposition high temperature (above 750°C) anneal treatment relieved some of the intrinsic stress created by lower temperature deposition (300 °C). This was attributed to volume reduction due to grain growth resulting in change in stress from compressive to tensile upon high temperature anneal. However, in addition the stress was reduced to 112.5 MPa at 600 °C as compared to a minimum stress of 311 MPa at 600 °C for LPCVD. This may be the result of a partial cancellation of the strong tensile thermal stress seen in LPCVD W films (due to the difference in thermal expansion between the W film and the substrate) by the compressive stresses in PECVD that result from ion bombardment effects[81]. The fact that net stress reduction is maximized at higher temperatures (>500 °C) is consistent with the observation by Green et al[84] that plasma phenomenon controls the microstructure at increasing temperatures, while it is thermally controlled up to 350 °C. In the rf power study (figure 3.8), by increasing rf power at higher temperatures (constant 600° C), the net stress is lowered to

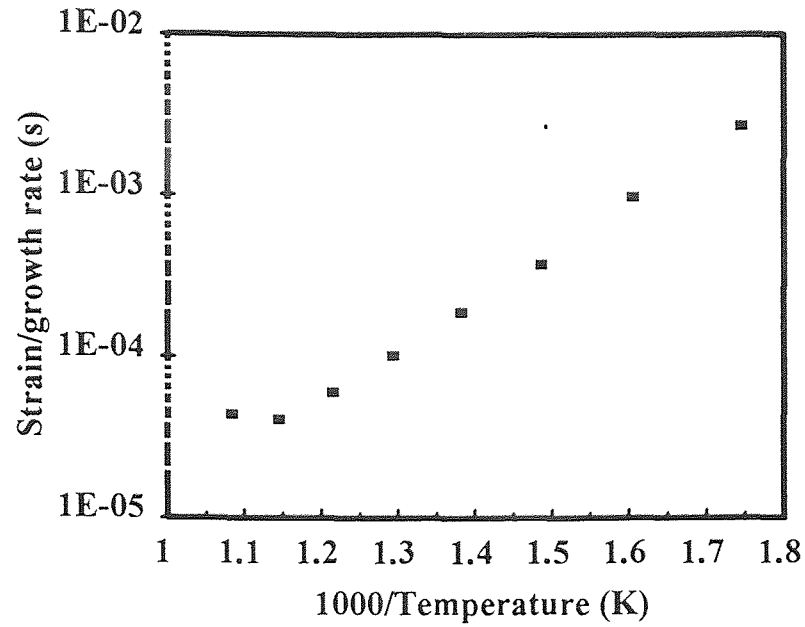


Figure 3.6 Variation of $\varepsilon\tau^{-1}$ as a function of reciprocal temperature

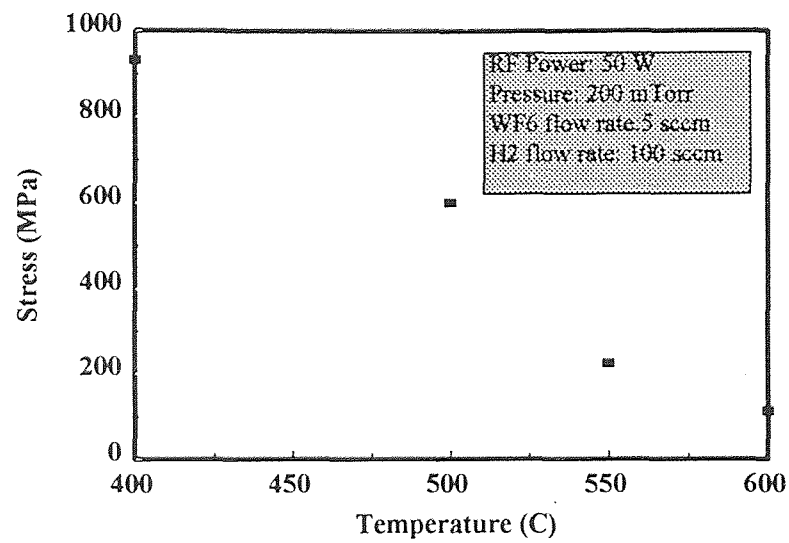


Figure 3.7 Variation of stress as a function of temperature at constant rf plasma power, pressure, WF₆ flow rate, and H₂/WF₆ flow rate ratio

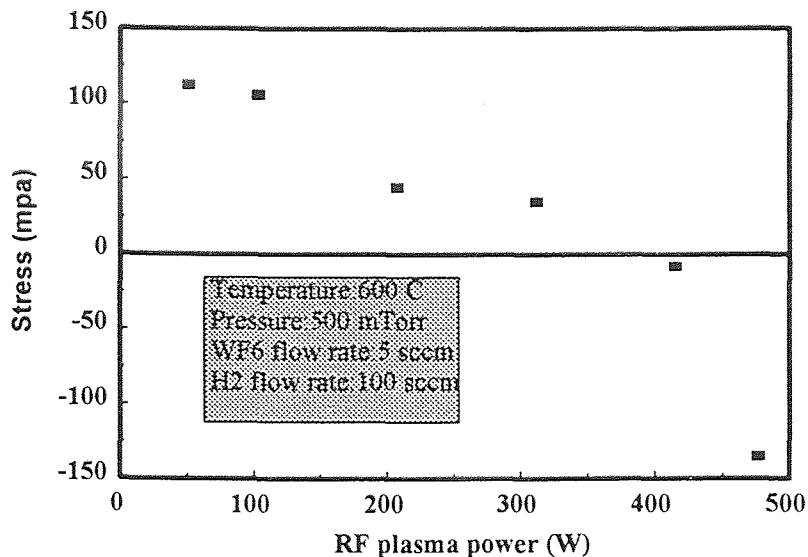


Figure 3.8 Variation of stress as a function of rf plasma power at constant temperature, pressure, WF_6 flow rate, and H_2/WF_6 flow rate ratio

zero and into the compressive regime. By tailoring the deposition parameters (rf power, temperature, pressure, and flow rate ratio etc.) it is shown that a film within a desired stress range, including a zero stress film, can be synthesized.

3.2.1.3 Pressure Effect: The pressure dependent behavior of stress is shown in figure 3.7, with the condition of a constant temperature ($500\text{ }^\circ\text{C}$) and flow ratio 20. The stress increase with the pressure. When the pressure increase, the deposition rate increase. From the buried layer (BL) model, We know the stress in the film is linearly with the deposition rate. So the pressure increase, the stress increase. But compared with the temperature effect, the pressure effect is not very strong.

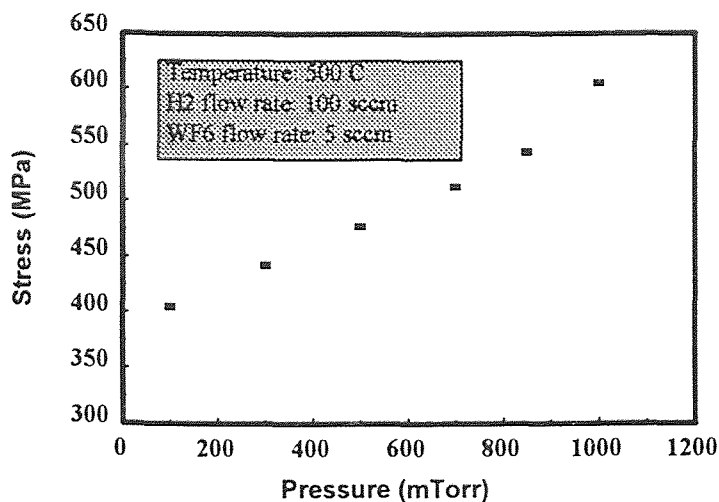


Figure 3.9 Variation of stress as a function of pressure at a constant temperature, WF₆ flow rate, and H₂/WF₆ ratio

3.2.1.4 Flow Rate Ratio Effect: The flow rate ratio effect on the film stress was studied on the constant WF₆ flow rate 5 sccm, temperature 500 °C, and pressure 500 mTorr. Before the ratio reach to 10, the stress increases quickly due to the deposition rate increase. After this ratio, the stress tend to keep as constant. From the kinetics study, we know the H₂ in the reaction chamber saturate at the high flow ratio and the stress no longer increase because of the constant deposition rate.

3.2.2 Resistivity

Another important application of the tungsten film is for interconnect material. The primary requirements for the interconnect material are low resistivity. This low resistivity can allow higher current density to be imposed on tungsten wiring with a

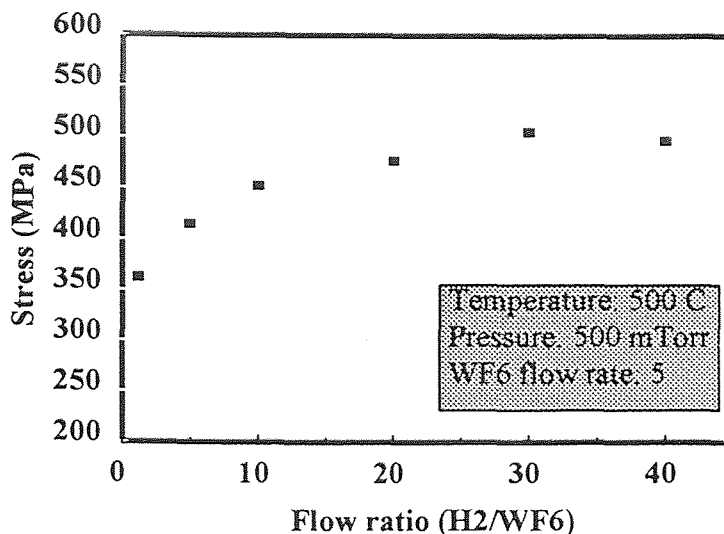


Figure 3.10 Variation of stress as a function of flow ratio at constant temperature, pressure and WF₆ flow rate

smaller line width, minimized interconnection or RC time delay of the device. Deposited tungsten film resistivities were calculated from sheet resistance values and film thickness. The film thickness values used were those calculated from the gravimetric, constant density analysis, for which a constant film density (19.3 g/cm^3) was assumed. In fact, the density of deposited tungsten film maybe is different from the bulk density. An accurate film thickness should be measured from SEM, stylus profilometer, etc[71]. Reported values for resistivities correspond to the measurement values. The resistivities were found to be higher than tungsten bulk resistivity, $5.3 \mu\Omega\text{-cm}$ at 20°C [33].

In order to investigate the resistivity further, three operation parameters (temperature, pressure and flow ratio) are considered as variables for the resistivity

studies. The three studies are based on the same condition as these parameters effect on stress study. These results are shown from figure 3.9 to figure 3.11 , and it is clear that the measured resistivity varies in a small range for both pressure and flow rate study series. The independent behaviors of pressure (100-1000 mTorr) series and flow rate (1 to 40) series can be determined. However, in temperature study series, shown in figure 3.9, the values of resistivity seems to increase at the lower deposition temperature from 350 to 300°C and decrease at the higher temperature. When W deposited at the lower temperature, the poorly connected grains of structure, and the electron scattering effect caused by phonons, impurities, vacancies, dislocations, grain boundaries, precipitated second phase particles, and compound phase [72] may be used as an explanations for low resistivity at low temperature. when deposited at high temperature, the grain size is large[54], this will result in the resistivity decreasing.

3.2.2.1 Resistivity of PECVD W Films: Resistivity of as-deposited tungsten films is dependent on all plasma parameters: resistivity decreases due to increasing rf power, temperature, and H_2/WF_6 ratio and with decreasing pressure and rf frequency[77]. Figs. 3.14 and 3.15 show the effects of rf plasma power and temperature respectively on resistivity. Increasing rf power is seen to reduce resistivity. This trend is consistent with enhanced desorption or sputtering of fluorine impurities from the surface via ion bombardment[36,77]. Increasing of temperature causes a small reduction in resistivity .The resistivity of all PECVD films regardless of parameter range appear to be as low or lower than those deposited by LPCVD. These low resistivities of as-deposited films may

be attributed firstly to the fact that deposition took place at temperatures high enough for only a-phase tungsten to be present, as in the case with all the LPCVD films. At temperatures below 300°C the mobility of tungsten may be too low to permit the nucleation and growth of the stable α -phase[85]. XRD analysis confirmed the presence of only a-phase tungsten film. For the rf power series a temperature of 600 °C was used. At these higher temperatures grain growth is increased, causing a further reduction in resistivity[86] coupled with the fact that as previously stated the microstructure is dominated by plasma phenomenon at higher temperatures. The plasma environment creates a non-equilibrium surface condition, in effect raising the effective surface temperature and with it enhanced grain growth. The effects of the plasma-surface interactions such as removal of fluorine from the surface as stated above or enhancement of tungsten subfluoride and hydrogen atom makes it possible to prepare PECVD tungsten films with resistivities as low or lower than LPCVD films deposited in the regime of the hydrogen reduction process[86].

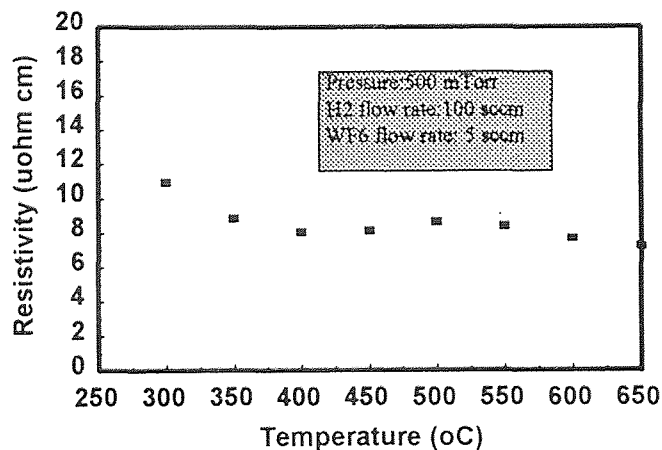


Figure 3.11 The dependent behavior of resistivity of CVD W on temperature

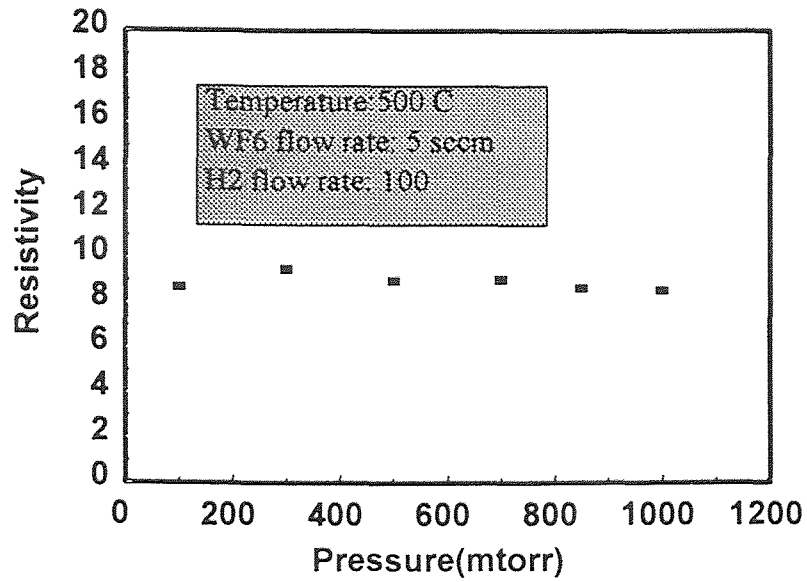


Figure 3.12 The independent behavior of resistivity of CVD W on total pressure

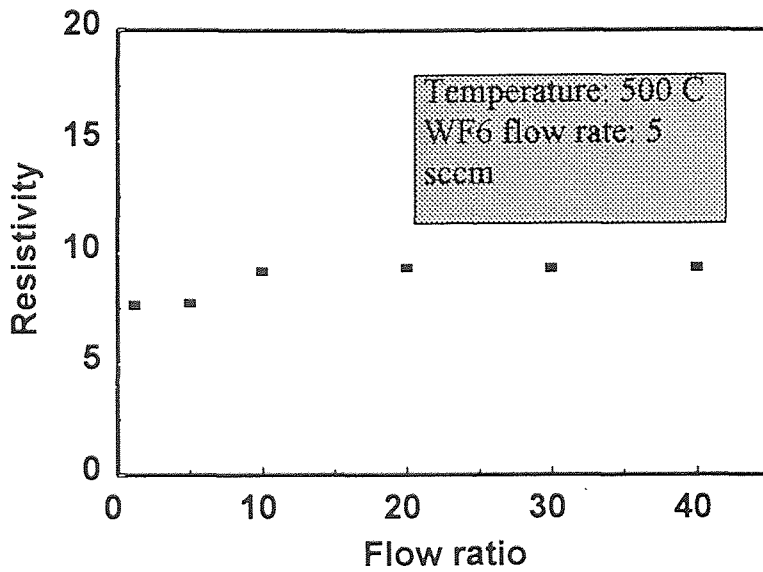


Figure 3.13 The independent behavior of resistivity of CVD W on flow ratio

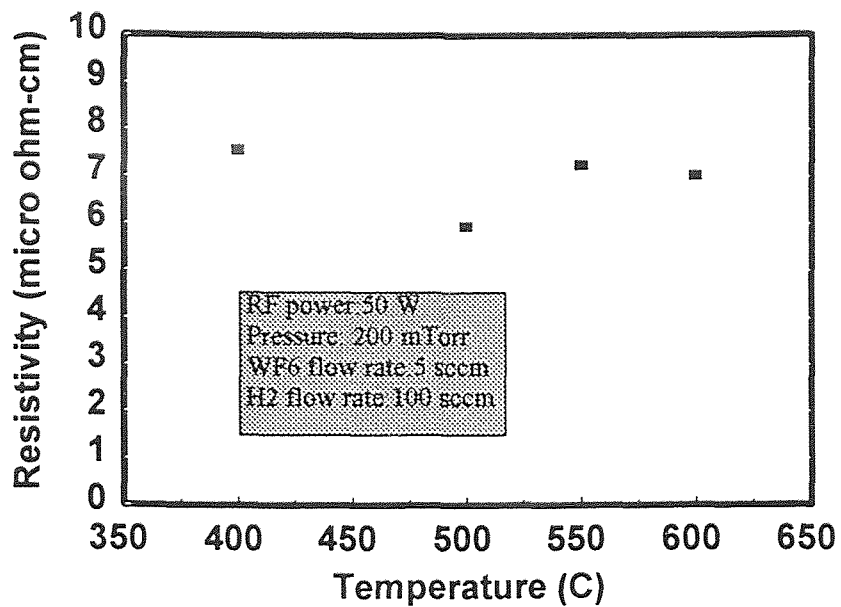


Figure 3.14 Resistivity as a function of rf plasma power

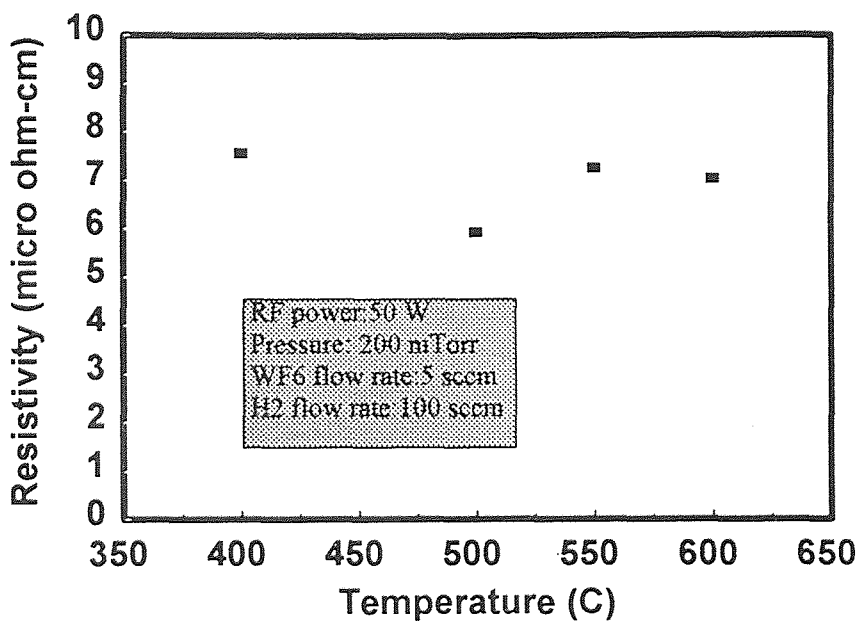


Figure 3.15 Resistivity as a function of temperature

3.2.3 Crystal Orientation

The types of phase and orientation of tungsten crystals formed by the deposition reaction were examined by X-ray diffraction analysis. The range examined for 2θ was between 30° and 80° , wide enough to identify α -W, β -W, and tungsten silicide phase. All the temperature series, pressure series and flow ratio series were measured by X-ray diffraction. No film was found to contain trace amount of β -W, whose characteristic peaks exist on $35.6, 40.04, 43.91, 64.17, 66.76, 70.17, 75.37 2\theta^\circ$ [73]. Figure 3.12 shows the typical X-ray diffraction pattern of tungsten film. Three α -tungsten characteristic peaks ($40.26, 58.27, \text{ and } 73.19 2\theta^\circ$) corresponding to lattice spacing ($2.238, 1.582, 1.292 \text{ \AA}$) are apparent in all the diffraction pattern.

The preferred orientation of the specific (hkl) plane can be evaluated by texture coefficient, TC (hkl) [74]:

$$TC(hkl) = \frac{I_m(hkl)}{I_r(hkl)} \bigg/ \frac{1}{n} \sum_{i=1}^n \frac{I_m(hkl)}{I_r(hkl)} \quad (3.11)$$

where $I_m(hkl)$ is the measured X-ray relative intensity of the (hkl) plane, $I_r(hkl)$ is the relative intensity in the powder pattern, and n is the total number of reflection peaks. Table 4 give the X-ray relative intensity of tungsten random powder[73].

The larger TC values mean a more markable orientation. If TC (hkl) is less than 1, the (hkl) plane has no preferred orientation. All the samples' TC (110) and TC (211) are less than 1 and TC (200) are larger than 1, so there is preferred orientation (200).

This is because the W (200) plane has same in-plane lattice geometry of square as the Si (100) plane, however, the W (110) has diamond in-plane lattice geometry[65]. The another reason is that the bcc tungsten is not closed packed and more open compared with (110) plane, the tungsten may be easy to adsorb on this open structure.

Figure 3.13 depicts the effect of deposition temperature on preferred orientation of (200). Between 300 to 400 °C, the preferred orientation of (200) increase with the temperature, then decrease quickly up to 500°C, after this the preferred orientation increase again. The temperature change will affect the adsorbate surface diffusion on the (200) and (110) plane, will affect the reconstruction of (200) plane [75], and will change the interface of Si/W. These factors all will affect the orientation of the films. It is these factors' inter balance that lead to this unique trend. R. Blumenthal, et al.[54] observed another phenomenon, the amount of (200) orientation decreases from 400-450°C, peaks at 500°C, and disappears as the temperature increases up to 650°C. This different result may be due to the different substrate. They coated Si wafer with SiO₂ and TiW layer. It is known the lattice match between the substrate and the growing film will determine the crystal orientation.

The pressure effect on the texture coefficient of (200) plane is shown on Figure 3.14. The preferred orientation of (200) plane increase with pressure followed by a constant trend. But this trend is not remarkable compared with that of the temperature dependency because the TC (200) kept in a small range between 1.4 to 1.6.

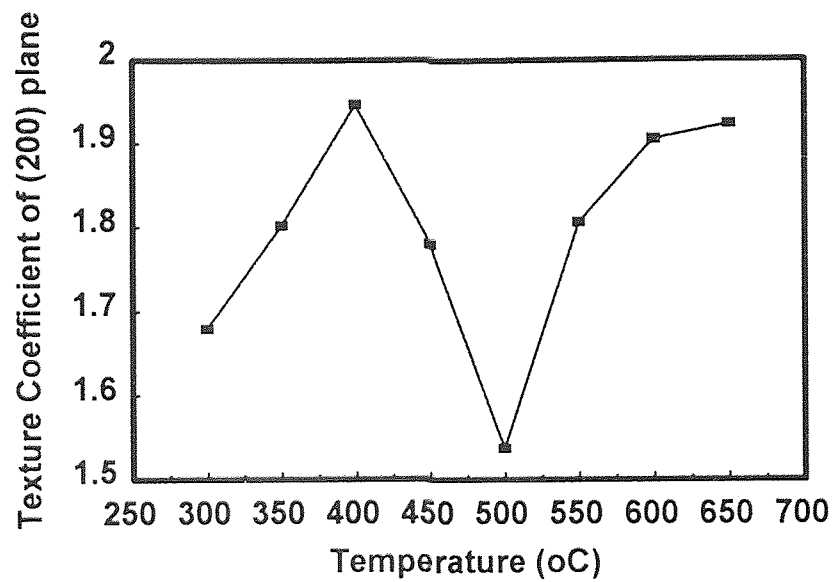
The flow ratio has a strong relationship with TC (200) which is shown on Figure 3.15. The preferred orientation of (200) plane decrease quickly with flow ratio than tend

to keep as constant at high flow ratio. This relationship is exactly opposite to the relationship between flow ratio and growth rate. We can not attribute the effect of flow ratio on TC (200) behavior to deposition rate because in the pressure series we find the opposite trend is formed. The reason which lead to this behavior is that more hydrogen which occupy the sites on the tungsten (200) plane will prevent the W adsorbing on this plane, then (200) plane orientation will decrease.

3.2.3.1 Crystal Orientation of PECVD Films: All PECVD-deposited tungsten films contained only a-W phase, consistent with studies employing PECVD performed at the temperature range used (400-600°C)[85-88]. All the samples in the rf power series at a constant temperature of 600°C displayed a marked preferred orientation of the (200) plane with TC's (200) greater than 15. This is greater than TC (200) for LPCVD at 600°C which was approximately 1.9. However the temperature series, while displaying a somewhat similar trend as LPCVD films of TC(200) with increasing temperature, had a TC(200) <1 for temperatures 500 and 550. As stated above, all LPCVD samples displayed a TC(200) >1 and a (200) plane preferred orientation. Since plasma-surface interactions may create changes in stress and resistivity due to microstructure changes from the LPCVD films, this would be reflected by changes in the relative intensities of the a-W peaks. In addition, fluctuations in rf power during these runs may have altered deposition conditions to effect film orientation.

Table 4. X-ray diffraction lines for α -W from random tungsten powder

plane	lattice spacing (\AA)	relative intensity	2θ
110	2.238	100	40.26
200	1.582	15	58.27
211	1.292	23	73.19

**Figure 3.16** Temperature effect on texture coefficient of (200) plane

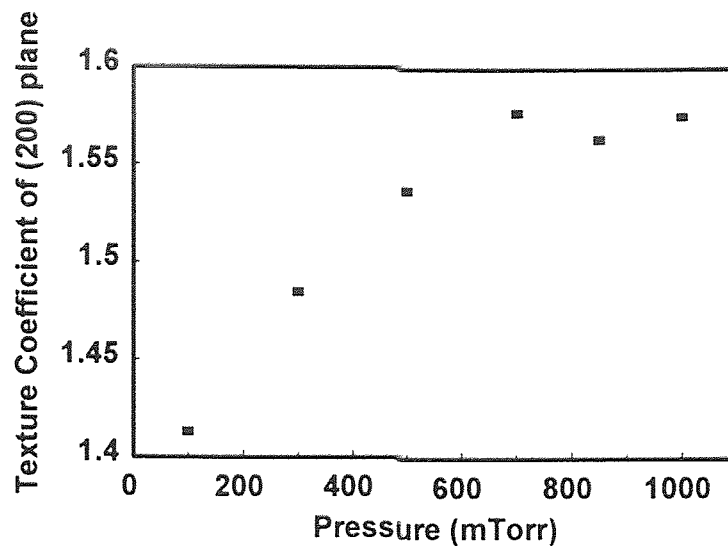


Figure 3.17 Pressure effect on texture coefficient of (200) plane

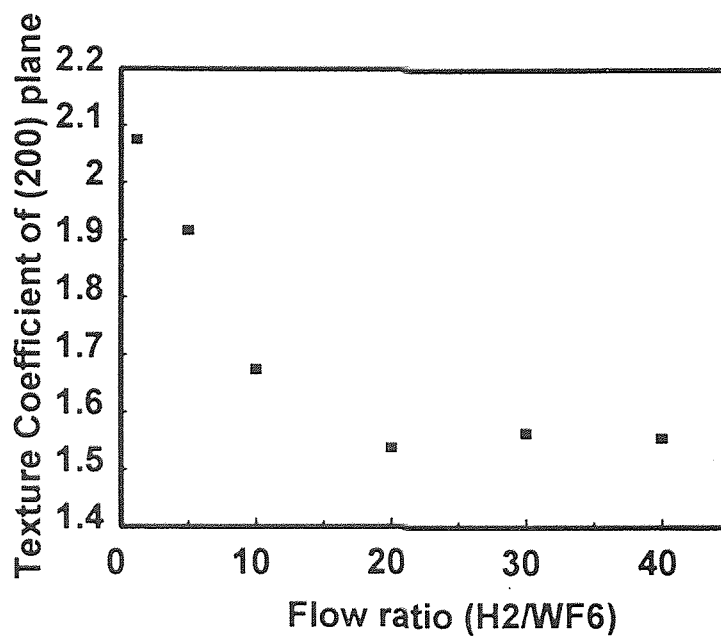


Figure 3.18 Flow ratio effect on texture coefficient of (200) plane

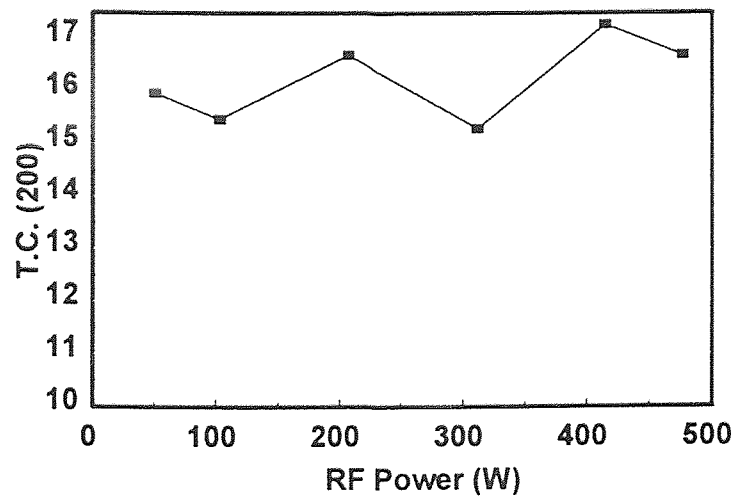


Figure 3.19 RF plasma power effect on texture coefficient of (200) plane

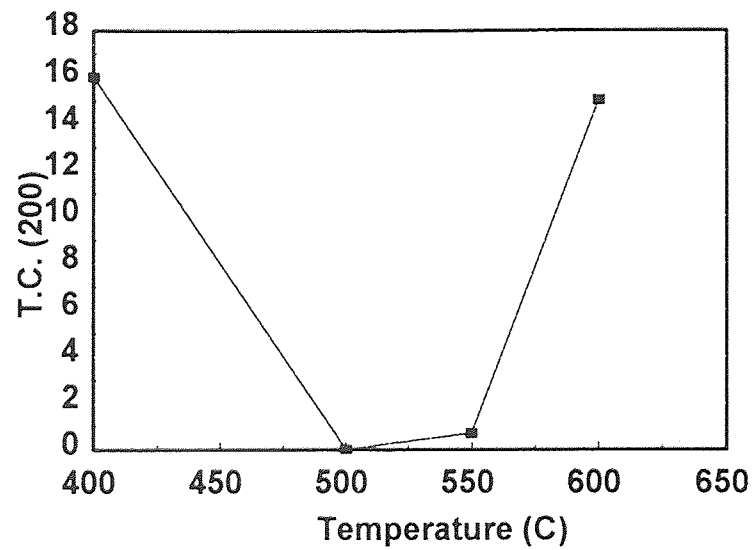


Figure 3.20 Temperature effect on texture coefficient of (200) plane of plasma films

CHAPTER 4

CONCLUSIONS AND SUGGESTIONS

This research included the fabrication and characterization of CVD tungsten film from H_2 and WF_6 for X-ray absorber in X-ray lithography technology.

Low stress films have successfully been synthesized on pure silicon wafers in a cold wall, single wafer reactor by low pressure chemical vapor deposition from H_2 and WF_6 in the temperature range of 300-650 °C, pressure range of 100-1000 mTorr, flow ratio range of 1-40. The growth kinetics were determined as a function of temperature, pressure and flow ratio. The deposition rate as deposited films was found to follow an Arrhenius behavior in the range of 300-500°C with an activation energy of 55.7 kJ/mol. The growth rate was seen to increase linearly with total pressure and H_2 partial pressure. In the H_2/WF_6 flow ratio studies conducted at 500°C and 500 mTorr, growth rate increase with flow ratio when flow ratio is lower than 10 followed by saturation above this ratio. The stress of deposited film strongly dependent on temperature and has weak relationship with pressure and flow ratio. These three parameters effect on stress can be explained by buried layer model which show the stress of as deposited film linearly dependent on growth rate factor and exponentially dependent on temperature factor. Low resistivity values (less than 10 $\mu\Omega \cdot cm$) were obtained for as-deposited condition. The pressure and flow ratio seem no effect on resistivity but resistivity is lower at high temperature and higher temperature. The X-ray diffraction patterns indicate the

$\langle 200 \rangle$ has preferred orientation in all as deposited films. The preferred orientation increase with temperature from 300 to 400 °C, then decrease up to 500°C, then increase again. The preferred orientation increase with pressure followed by constant at high pressure. But the preferred orientation decrease with flow ratio then tend to keep at constant at high flow ratio.

However, this study still did not synthesize free stress film. Some improvement must be done which include:

(1) Wafer treatment:

Some researches show the major stress in the CVD tungsten film come from the reaction interface of W/Si, So preventing the reaction in the interface between Si and W can reduce the stress. This can be realized by first depositing TiN at the Si wafer. This TiN layer not only can reduce the stress but also can improve the W adhesion to the substrate.

We deposit the W on the Si wafer, but Si is not a good material for X-ray mask membrane. We had better deposit W on the SiC or SiN substrate. Because the different substrate will lead to different nucleation it is expected to obtain the different optional W deposition condition.

(2) Plasma CVD process conditions:

Plasma enhanced chemical vapor deposition of W can get the compressive stress but low pressure chemical vapor deposition of W can get the tensile stress. If we can combine these two processes, maybe we can get the free stress film.

(3) Reduction agent development:

There are several chemicals which can be used to reduce WF_6 precursor. Silane is one of the candidates in that it will suppress the reaction between W and Si. We should explore the stress if plasma-enhanced deposited from the silane using Spectrum 211.

(4) Anneal as deposited film

Annealing the as deposited film will decrease the stress in the film. We should try to use the method and find the mechanism of this method.

4.1 Conclusions and Suggestions-PECVD Study

The achievement of zero stress, low resistivity tungsten films on pure silicon wafers has been achieved with the PECVD process. By increasing RF plasma power at constant deposition parameters (pressure: 500 mTorr, temperature: 600 °C, constant WF_6 and H_2 flow rates, 5 and 100 sccm respectively) the stress was seen to change from compressive down to zero at approximately 400 W RF power and into the tensile regime at maximum RF power of 500 W. As stated previously, by varying plasma parameters this permits the synthesis of not only zero stress film for use in X-ray lithography applications also other potential applications where a desired intrinsic stress within the stress range of tungsten films produced in this study are required. In addition, the resistivity was as low or lower than LPCVD films, with only α -phase tungsten present. This precludes the need for a post-deposition treatment anneal or the use of alternate precursor development as a means of reducing stress and/or resistivity. Deposition with a sufficiently high degree of thermal activation (deposition temperature 600 °C) that minimized stress by this means alone enhanced by a suitably strong enough plasma environment was the means to

successfully achieve the goal of stress-free tungsten film that was not reached in the LPCVD study.

REFERENCES

1. A.Heuberger, *J.Vac.Sci.Technol.*, **B6(1)**, 107 (1988).
2. R.A.Colclaser, *Microelectronics:Processing and Design*, J.Wiley and Sons, Inc., New York, (1980).
3. Alan.D.Wilson, *SPIE 537, Electron-Beam, X-Ray, and Ion-Beam Techniques for Submicrometer Lithographies IV*, 85 (1985).
4. A.Heuberger, *Solid State Technology*, **2**, 93 (1986).
5. A.R.Shimkunas, *Solid State Technology*, **9**, 192 (1984).
6. Aubrey Tobey, *Microelectronic Manufacturing and Testing.*, **6**, 35 (1987).
7. A.W.Yanof, D.J.Resnick, C.A. Jankoski, and W.A.Johnson, *Proceedings of the SPIE*, Santa Clara, CA, P.D.Blais Ed., 632 (1986).
8. H.Betz, H.-I.Huber, S. Pongratz, W.Rohrmoser, and W. Windbracke, *Microelectron. Eng.*, **5**, 41 (1986).
9. I.Plotnik, M.E.Porter, M.Toth, S.Akhtar, and Henry I. Smith, *Microelectronic Engineering*, **5**, 51 (1986).
10. M.Karnezos, R.Ruby, B.Heflinger, H.Nakano, and R.Jones, *J.Vac.Sci.Technol.*, **B5**, 283 (1987).
11. A.M.Gosnet and F.R.Ladan, *Microelectron Eng.*, **6**, 253 (1987).
12. Yao C. Ku and Henryl. Smith, *J.Vac.Sci.Technol.*, **B6(6)**, 2174 (1988).
13. H.Luethje, M.Harms, A. Bruns,and V.Mackens, *Microelectron. Eng.*, **6**, 259 (1987).
14. Nobuyuki Yoshioka, Susumu Takeuchi, Hiroaki Morimoto and Yaichiro Watakabe, *SPIE, Electron-Beam X-ray, and Ion-beam Technology. Submicrometer Lithographies VII*, 923 (1988).
15. W.Kern, Chemical Vapor Deposition, *Microelectronic Materials and Processes*, R.A.Levy Ed., Kluwar Academic, New Jersey, 203 (1986).
16. D.W.Shaw, *Crystal Growth*, C.H.L.Goodman Eds, Plenum Press, London, 1, (1974).

17. S.Wolf and R.N.Tauber, *Silicon Processing for the VLSI Era*, Lattice Press, California, 110 (1986).
18. Laidler, K.J, *Chemical Kinetics*, Harper & Row, New York, 267 (1987).
19. A.W.Vere, *Crystal Growth Principles and Progress*, Plenum Press, New York,
20. A.Reisman and M.Berkenblit, *J.Electrochem. Soc.*, **113**, 146 (1966).
21. S.Wolf and R.N.Tauber, *Silicon Processing for the VLSI Era*, Lattice Press, California, 124 (1986).
22. H.C.Theurer, *J.Electrochem. Soc.*, **108**, 649 (1961).
23. W.Kern and V.S.Ban, *Thin Film Processes*, J.L.Vossen and W.Kern, Eds., Academic Press, New York, (1978).
24. W.Kern and G.L.Schnable, *IEEE Trans.Electron Devices*, **ED-26**, 647 (1979).
25. R.S.Rosler, *Solid State Technol.*, **20(4)**, 63 (1977).
26. A.R.Reinberg, *Annu.Rev. Mater.Sci.*, **9**, 341 (1979).
27. T.Sugano, *Application of Plasma Processes to VLSI Technology*, John Wiley & Sons, New York ,(1985).
28. J.W.Peters, F.L.Gebhart, and T.C.Hall, *Solid State Technol.*, **23(9)**, 121 (1980).
29. J.W.Peters, *IEEE-IEDM Tech.Dig.*, 240 (1981).
30. S.D.Allen, A.B.Trigubo, and Y.-C.Liu, Chemical Vapor Deposition, *The Electrochemical Society*, J.M.Blocher Jr., G.E.Vuillard, and G.Wahl, Eds., Pennington, New Jersey, 267 (1981).
31. Y.Kusumoto, K.Takakuwa, H.Hashinokuchi, T.Ikuta, and I.Nakayama, *Tungsten and Other Refractory Metals for VLSI Applications III*, V.A.Wells, Ed.,MRS Publishers, Pittsburgh, Pennsylvania, 3 (1988).
32. J.Randall Creighton and J.E.Parmeter, *Critical Reviews in Solid State and Materials Sciences*, **18(2)**, 175, (1993).
33. R.A.Levy and M.L.Green, *J.Electrochem. Soc.*,**134(2)**, 37 (1987).
34. M.Diem, M.Fisk, and J.Goldman, *Thin Solid Films*, **107**, 39 (1983).

35. Y.Kusumoto, K.Takakuwa, H.Hashinokuchi, T.Ikuta and I.Nakayama, *Tungsten and Other Refractory Metals for VLSI Applications III*, V.A.Wells, Ed., MRS Publishers, Pittsburgh, Pennsylvania, 103 (1988).
36. Mehrdad M.Moslehi, *ibid*, 385.
37. E.K.Broadbent, and C.L.Ramiller, *J.Electrochem.Soc.*, **131**, 1427 (1984).
38. N.Lifshitz, *Tungsten and Other Refractory Metals for VLSI Applications III*, V.A.Wells, Ed., MRS Publishers, Pittsburgh, Pennsylvania, 83 (1988).
39. M.L. Green, Y.S.Ali, T.Boone, B.A. Davidson, L.C.Feldman, and S.Nakagara, *Tungsten and Other Refractory Metals for VLSI Application II*, E.K.Broadbent, Ed., MRS Publishers, Pittsburgh, Pennsylvania, 85, (1986).
40. M.E.Tracy, *Tungsten and other Refractory Metals for VLSI Applications*, R.S.Blewer, Ed., MRS Publishers, Pittsburgh, Pennsylvania, (1985).
41. R.V.Joshi, D.A.Smith, S.Basavaiah, and T.Lin, *Tungsten and Other Refractory Metals for VLSI Applications III*, V.A.Wells, Ed., MRS Publishers, Pittsburgh, Pennsylvania, 39 (1988).
42. K.Y.Tsao and H.H.Busta, *J Electrochem. Soc.*, **131**, 2702 (1984).
43. C.M.McConica and K.Krishnamani, *J.Electrochem.Soc.*, **133**, 2542 (1986).
44. E.K.Broadbent and C.L.Ramiller, *J.Electrochem.Soc.*, **131**, 1427 (1984).
45. R.V.Joshi, D.A.Smith, S.Basavaiah, and T.Lin, *Tungsten and other Refractory Metals for VLSI Applications*, R.S.Blewer, Ed. MRS Publishers, Pittsburgh, Pennsylvania, 39,(1985).
46. J.R.Creighton, *J.Vac.Sci. Technol.*, **A7**, 621 (1989).
47. A.M.Shroff and G.Delval, *High Temperatures-High Pressures*, **3**, 695 (1971).
48. R.A. Levy and M.L.Green, *Mat.Res.Soc.Symp.Proc.*, **71**, 229 (1986).
49. M.R.McLaury, R.W.Stoll, and D.W.Woodruff, *Tungsten and other Refractory Metals for VLSI Applications*, R.S.Blewer, Ed., MRS Publishers, Pittsburgh, Pennsylvania, 467 (1985).
50. W.T.Stacy, E.K.Broadbent, and M.H.Norcott, *J. Electrochem. Soc.*, **131**, 444 (1985).

51. J. Weissman and M.C. Kinter, *J. Am. Phys. Soc.*, **34**, 3187 (1963).
52. T.I. Kamins, D.R. Bradbury, T.R. Cass, S.S. Laderman, and G.A. Reid, *J. Electrochem. Soc.*, **133**, 2555 (1986).
53. R.V. Joshi, E. Mehter, M. Chow, M. Ishaq, S. Kang, P. Geraghty, J. McInerney, *Tungsten and Other Advanced Metals for VLSI/ULSI Applications V*, S.S. Wong and S. Furukawa, Eds, MRS Publishers, Pittsburgh, Pennsylvania, 157 (1990).
54. R. Blumenthal, G.C. Smith, H.Y. Liu and H.L. Tsai, *ibid.*, 65.
55. T. Ohba, T. Suzuki, T. Hara, Y. Furumura, and K. Wada, *ibid.*, 17.
56. J.E.J. Schmitz, A.J.M. van Dijk, and M.W.M. Graef, *Proc. Of the 10th Int. Conf. On CVD*, G.W. Cullen, Ed, Electrochem. Soc., Princeton, New Jersey, **87**, 625
57. N. Kobayashi, H. Goto, and M. Suzuki, *Proc. of 11th International Conf. CVD*, Electrochem. Soc., Princeton, New Jersey, 434 (1990).
58. C.A. Van der Jeugd, A.H. Verbruggen, G.J. Leusink, G.C.A.M. Janssen, and S. Radehar, *Tungsten and Other Advanced Metals for VLSI/ULSI Applications V*, S.S. Wong and S. Furukawa, Eds, MRS Publishers, Pittsburgh, Pennsylvania, 267 (1990).
59. M. Suzuki, N. Kobayashi, and K. Mukai, *ibid.*, 259.
60. S. Sivaram, M.L.A. Dass, C.S. Wei, B. Tracy, and R. Shukla, *J. Vac. Sci. Technol.*, **A11(1)**, 87, (1993).
61. J.E.J. Schmitz, A.J.M. Van Dijk, and M.W.M. Graef, *Proc. Of the 10th Int. Conf. On CVD*, G.W. Cullen, Ed, Electrochem. Soc., Princeton, New Jersey, **87**, 625
62. M. Saitoh, T. Nishoida, M. Suzuki, N. Kobayashi, and T. Kure, *Tungsten and Other Advanced Metals for VLSI/ULSI Applications V*, S.S. Wong and S. Furukawa, Eds, MRS Publishers, Pittsburgh, Pennsylvania, 201 (1990).
63. Takayuki Ohba and Shin-ichi Inoue, *ibid.*, 281.
64. Takashi Akahori, Takayuki Tani, and Satoshi Nakayama, *Tungsten and Other Advanced Metals for VLSI/ULSI Applications V*, S.S. Wong and S. Furukawa, Eds, MRS Publishers, Pittsburgh, Pennsylvania, 209 (1990).
65. Oktay H. Gokce, Ph.D. Thesis, *Kinetics of the Tungsten Hexafluorine-Silane Reaction for the Chemical Vapor Deposition of Tungsten*, Montana State University, Bozeman, Montana (1991).

66. L.I. Maissel, *Handbook of Thin Film Technology*, L.I. Maissel and R. Glang, Eds McGraw-Hill, New York, 1, (1970).
67. Stoney, G.G. *Proc.R.Soc.*, London, **A82**, 172 (1909).
68. E.Kloholm and B.S.Berry, *J.Electrochem.Soc.*, **115**, 823 (1968).
69. G.J.Leusink, T.G.M.Oosterlaken, G.C.A.M.Janssen, and S.Radelaar, *J. Appl. Phys.*, **(6)**, 3899, (1993)
70. T.I.Kamins, D.R.Bradbury, T.R.Cass, S.S.Laderman, and G.A.Reid, *J.Electrochem. Soc.*, **133(12)**, 2555 (1987).
71. Milton Ohring, *The Materials Science of Thin Films*, Academic Press, Inc. San Diego, California (1992)
72. Do-Heyoung Kim, Robert H.Wentorf, and William N.Gill, *J.Electrochem.Soc.*, 3273 (1993).
73. *X-ray Powder Data File*, J.V. Smith, Ed., American Society for Testing and Materials, Philadelphia, (1960).
74. M.S.Kim and J.S.Chun, *Thin Solid Films*, **107**, 29 (1983).
75. J.M.MacLaren, J.B. Pendry, P.J.Rous, D.K.Saldin, G.A.Somorjai, M.A.Van Hove, and D.D.Vvendensky, Surface Crystallographic Information Service. Handbook of Surface Structures, Reidel Publishing Company, Dordrecht, Holland (1988)
76. Michael L. Hitchman and Klavs F. Jensen. *Chemical Vapor Deposition Principles and Applications*, Academic Press, New York, (1993)
77. D.W.Hess, *Tungsten and Other Refractory Metals For VLSI Applications*, R.S. Blewer, Ed., MRS Publishers, Pittsburgh, Pennsylvania, 105 (1986)
78. S.V.Nguyen, *J.Vac.Sci.Technol.B*, **4(5)**, 1159 (1986)
79. K.Akimoto and K.Watanabe, *Appl.Phys.Lett.*, **39(5)**, 445 (1981)
80. J.Wood, *Applied Surface Science*, **38**, 397 (1989)
81. A.Belkacem, Y.Arnal, J.Pelletier, E.Andre, and J.C.Oberlin, *Thin Solid Films*, **241**, 301 (1994)
82. H.L.Park, C.D.Park, and J.S.Chun, *Thin Solid Films*, **166**, 37 (1988)

83. Man Wong and Krishna C. Saraswat, *Tungsten and Other Refractory Metals For VLSI Application IV*, R.S.Blewer and C.M.McConica Eds, MRS Publishers, Pittsburgh, Pennsylvania, 291 (1989)
84. W.M.Green, D.W.Hess, and W.G.Oldham, *J.Appl.Phys.*, **64(9)**, 4696 (1988)
85. C.C.Tang and D.W.Hess, *Appl.Phys.Lett.*, **45(6)**, 633 (1984)
86. Yong Tae Kim, Suk-Ki Min, Jong Sung Hong, and Choong Ki Kim, *Appl.Phys.Lett.*, **58(8)**, 837 (1991)
87. Jong-Sung Hong, Yong Tae Kim, Suk-Ki Min, Tae Won Kang, and Chi Yhou Hong, *J.Appl.Phys.*, **70(4)**, 2366 (1991)
88. Yong Tae Kim, Suk-Ki Min, Jong Sung Hong, and Choong -Ki Kim, *Jpn.J.Appl.Phys.*, **30(4)**, 820 (1991)